

LEGAL NOTICE

This report was prepared as an account of Government sponsored work. Neither the United States nor the Commission, and any persons acting on behalf of the Commission, make any warranty, representation, expressed or implied, with respect to the accuracy, completeness, or usefulness of the information contained in this report, or that the use of any information, apparatus, method, or process disclosed in this report may not infringe on existing or pending rights.

It is advised that individuals with respect to the use of, or for damages resulting from the use of any invention, apparatus, method, or process disclosed in this report, should apply to the Patent Office for protection of their rights. The Commission and the Commission's staff members are authorized to reproduce and distribute reprints for Government purposes, not withstanding any copyright notation that may appear hereon.

BNWL-1051
 Part 3
 48
 UC-49

Biology and Medicine

PACIFIC NORTHWEST LABORATORY
 ANNUAL REPORT FOR 1968
 to the
 USAEC Division of Biology and Medicine
 VOLUME II: PHYSICAL SCIENCES
 Part 3. Instrumentation

by

N. S. Porter, Manager
 and
 Staff Members of
 Electronic Measurements Research Section
 Applied Physics Department

with

W. G. Spear, Manager
 and
 Staff members of
 Instrument Research and Development Section
 Control and Instrumentation Department

July 1969

0012010

BATTELLE MEMORIAL INSTITUTE
 PACIFIC NORTHWEST LABORATORY
 Richland, Washington 99352

BLANK PAGE

0012011

Volume I of this report to the USAEC Division of Biology and Medicine covering work in the biological and ecological sciences and water and land resources is issued as BNWL-1050, Parts 1 and 2. Volume II of this report covers work in the physical sciences and is issued in three parts: Atmospheric Sciences, BNWL-1051, Part 1; Radiological Sciences, BNWL-1051, Part 2; and Instrumentation, BNWL-1051, Part 3.

Printed in the United States of America
Available from

Clearinghouse for Federal Scientific and Technical Information
National Bureau of Standards, U.S. Department of Commerce
Springfield, Virginia 22151

Price: Printed Copy \$3.00; Microfiche \$0.65

0012012

TABLE OF CONTENTS

Wound Counting With Solid State Detectors - K. L. Swinth	1
Suppression of Partial Energy Deposition Events in a Solid State Detector - K. L. Swinth.	7
Development of Pulse Shape Discrimination Circuitry for Compton Suppression Applications - N. C. Hoitink and L. D. Philipp	13
Feasibility of Using Cross-Correlation Techniques to Determine <u>In Vivo</u> Radionuclide Location - T. H. Morton	18
Miniature Implantable High Voltage Supply - E. M. Sheen and R. I. Wilbur	22
Irradiation Effects on Charge-Multiplying Diode Detectors - N. C. Hoitink	25
Tritium Target Scanning Using Surface-Contoured Diodes: Preliminary Results - T. H. Morton	28
Radon Monitoring - K. L. Swinth.	30
Control System for <u>In Vivo</u> Neutron Activation of Short Half- Life Nuclides - E. M. Sheen.	35
Smoking Control for Canines - R. I. Wilbur	38
Publications and Presentations	44

PACIFIC NORTHWEST LABORATORY
ANNUAL REPORT FOR 1968
to the
USAEC Division of Biology and Medicine
VOLUME II: PHYSICAL SCIENCES
Part 3. Instrumentation

WOUND COUNTING WITH SOLID STATE DETECTORS

Lithium-drifted silicon detectors can be used to accurately measure (± 0.2 mm) the depth of typical point sources of plutonium, but distributed sources introduce large errors. The effects of line sources and surface contamination on depth estimation are presented.

Investigator:
K. L. Swinth

INTRODUCTION

Due to the great radiotoxicity of plutonium, accurate and rapid assessment of the quantity and location of plutonium material present in a wound must be made in order to determine a course of action. Most commonly a thin NaI(Tl) crystal mounted on a low-noise photomultiplier is used to locate the material in a wound.

However, a simple scintillation detector, although quite sensitive, does not give adequate information as to the location of imbedded material. Its use realizes reasonable X-Y resolution but no depth informa-

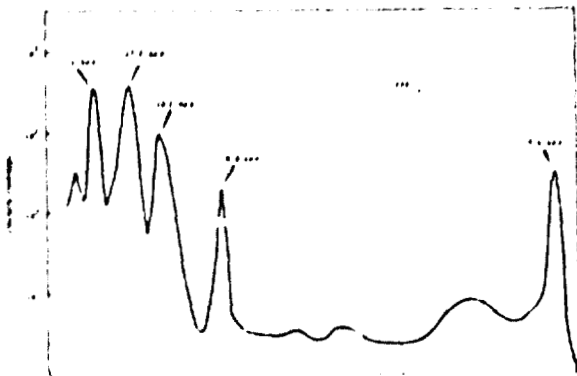
tion. Improper location of imbedded material prior to excision can result in further spread of the contaminant within the wound as well as unnecessary trauma.

The recent increase of interest in solid state detectors and improved performance at low energies suggest their use in wound counting. The lithium-drifted silicon or germanium detectors can resolve the L X rays of plutonium from which the depth of an imbedded source can be estimated by the differential absorption of the X rays. The general features of drifted detectors are discussed in relation to wound counting and they are compared to sodium

iodide and surface-contoured detectors.⁽¹⁾

DISCUSSION

^{239}Pu is generally detected by the emission of its daughter's three L X rays at 13.6, 17.2, and 20.2 keV. At these energies the absorption coefficient of tissue varies rapidly and the relative intensities of the X rays give an indication of the amount of interposed tissue. Presently used NaI(Tl) detectors will not resolve these X rays; however, using solid-state detectors with cooled preamplifiers produces fine resolution such as that shown in Figure 1. The system resolution is 0.7 keV and 0.8 keV full width at half maximum (FWHM) for the ^{241}Am (daughter of ^{241}Pu) gamma rays at 26.4 keV and 59.6 keV, respectively.

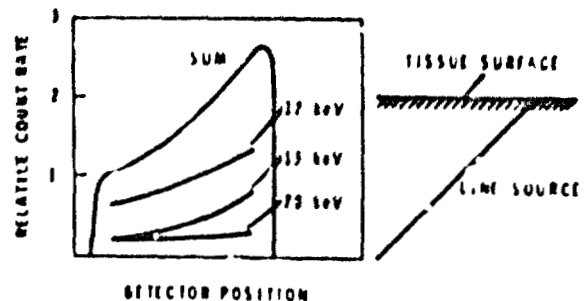


Neg 0682155-14

FIGURE 1 - Plutonium Spectrum
From 10 keV to 70 keV

These gamma rays, present in all plutonium samples, produce intensities varying with the sample irradiation history and time since separation.⁽²⁾ Although not resolved from the ^{239}Pu X-rays, ^{241}Am also emits L X rays. This causes the X-ray intensity to vary with isotopic composition.

Figure 2 shows the calculated intensity of the X rays above a 1 cm uniform line source imbedded in tissue at an angle of 45° . One can see the variation in intensity of the three X rays with depth. This variation can be used to estimate the average depth of a source after a method first described by H.E. Palmer, et al.⁽³⁾ The depth of the line source may be measured (calculated) as 1 mm less than an equivalent point source placed at the average geometrical depth. This results in an under-estimation of the



Neg 0682155-2

FIGURE 2 - Calculated Intensity
Variation Above a Line Source
Imbedded at 45° in Tissue

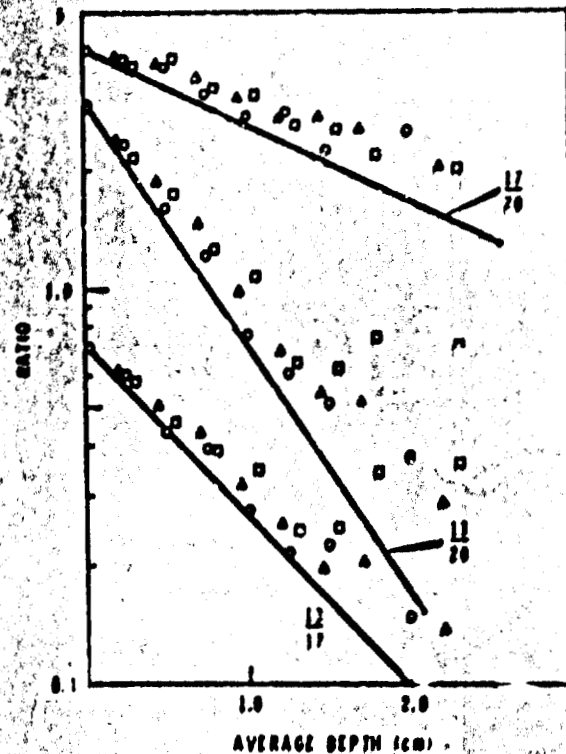
0012015

amount present by about 8% when compared to an equivalent point source.

By experiment and calculation we attempted to relate the effect of distributed sources on the determination of the depth and quantity of deposited material in wounds. For the experimental work, line sources utilizing a ^{239}Pu solution in a 23 mil inside diameter polyethylene tube were placed in a water phantom at various depths and angles. Sources of this geometry were used because they were easy to make and seemed to be a reasonable simulation of fine slivers of metal. The sources exhibited an activity of about 0.10 μCi . Even though the background rate from 10 keV to 70 keV was only 20.7 cpm, the low geometrical efficiency made it necessary to use 20 minute or longer counting periods. The background rates at the X-ray energies were 1.2 counts/min. at 13.2 keV, 1.4 cpm at 17.2 keV and 1.0 cpm at 20.2 keV.

RESULTS

Figure 3 shows results obtained with a 0.5 cm line source inclined at 0°, 45°, and 90° to the horizontal. The cpm ratios of the $\frac{13 \text{ keV}}{20 \text{ keV}}$, $\frac{17 \text{ keV}}{20 \text{ keV}}$, and $\frac{13 \text{ keV}}{17 \text{ keV}}$ X rays are plotted on the figure against the average geometrical depth. Although not apparent on this figure, a slight



Neg 882155-4

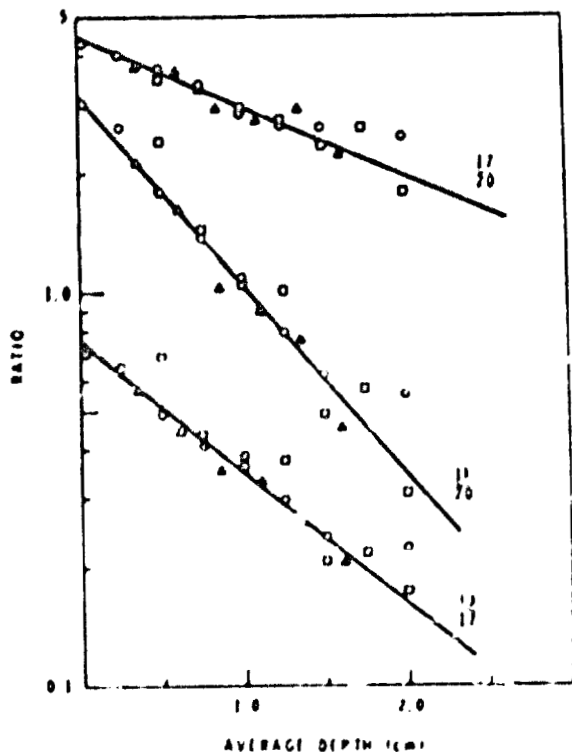
FIGURE 3 - Variation of X-Ray cpm Ratios of 0.5 cm Line Sources vs. Depth

increase in the X intercept with average depth could be detected. Tests with line sources up to 3 cm in length indicated an increase in the intercept, or separation of the exponential curves, with increasing geometrical length. However, no significant change in the slope of the ratios was noted and using the average exponential length rather than the geometrical length brought the curves into coincidence.

For purposes of simplicity, the average geometrical length is adequate to determine depth for source lengths up to about 1 cm. Note that

0.87 cm separate the 13/20 curves for a point and 3 cm line sources while the separation between a 1 cm line source and point source is less than 0.25 cm but greater than the 0.1 cm indicated by previous calculations. The effect is less for the other ratios.

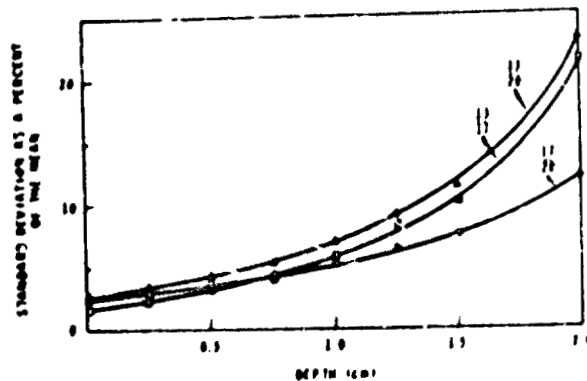
Figure 4 shows results similar to Figure 3 for a 1 cm line source. Statistical deviations do not appear on the previous figures; however, one does need to know something about the statistical errors in order to evaluate the method. Figure 5 shows the standard deviation



Neg 682155-5

FIGURE 4 - Variation of X-Ray opm Ratios For a 1.0 cm Line Source vs. Depth

0012017



Neg 682155-9

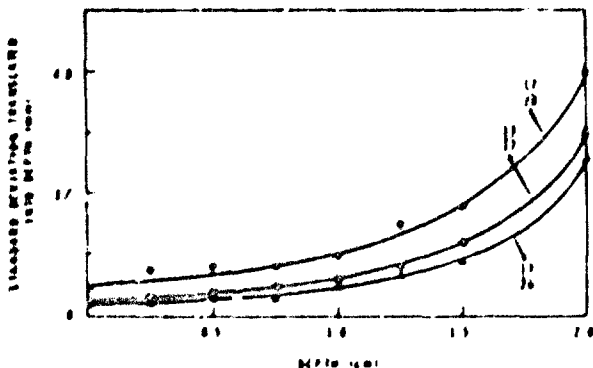
FIGURE 5 - Standard Deviations for the Three X-Ray opm Ratios as a Function of Depth

of the ratio plotted as a percent of the mean ratio for a 0.5 cm line source of 0.145 μ Ci counted in a horizontal position for 20 minutes. The ratio of the 17/20 keV X rays appears to be statistically better except at low energies where the ratio of the 13/17 keV X rays becomes more favorable. This needs to be interpreted in light of the slopes of the ratio curves. Figure 6 shows the standard deviation in mm as interpreted from the slope of the ratios. We now see that the ratio of the 13/20 keV X rays is uniformly more favorable as long as there are enough counts in the X-ray peaks. This figure indicates that the material imbedded at an average depth of less than 5 mm can be located with an accuracy of ± 0.5 mm in 95% of the cases. The same relative accuracy may be obtained up to depths

of about 1 cm, but beyond this the accuracy deteriorates rapidly. One must recall that a deviation greater than the statistical error is caused by the effect of using the geometrical average depth for line sources.

Surface contamination or similar changes in the distribution of activity with depth causes important errors in the estimation of effective depth. With an equivalent amount of surface contamination present, a 1 cm long source at 45° with a normal average geometrical depth of 0.37 cm, will have a measured depth of 0.15 cm.

Figure 7 shows the sensitivity variation with depth for the ²⁴¹Am gamma ray (60 keV) and for the sum of the three X rays. As noted on the figure, variations in both depth and geometry occur. Using the data



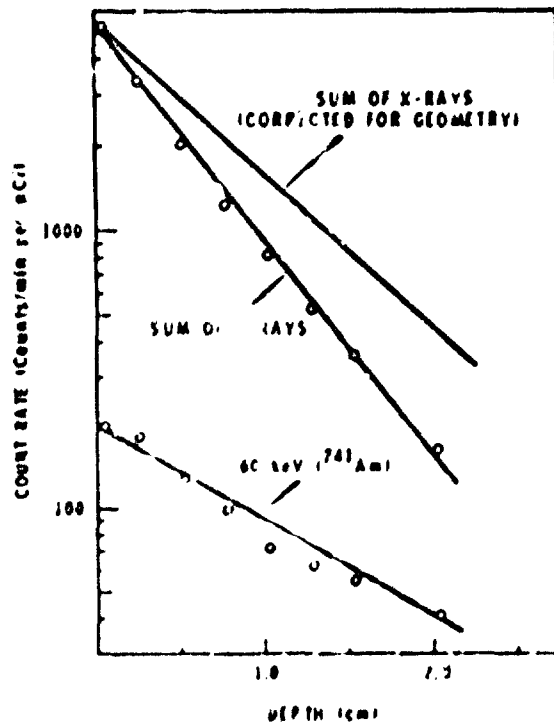
Neg 682155-8

FIGURE 6 - Standard Deviation for the Three Ratios Translated Into Standard Deviations in Depth vs. Depth

shown on this figure we can calculate a "Minimum Detectable Amount" (MDA)⁽¹⁾ of 0.25 nCi for surface contamination and 8.5 nCi for activity at 2.0 cm depth. Of course at these levels it would not be possible to use the ratio of the cpm of the X rays because of statistical considerations.

SUMMARY AND CONCLUSIONS

For wound counting, one needs a detection unit which will rapidly show the location and amount of material in a manner which can be easily interpreted. It must be able to



Neg 682155-7

FIGURE 7 - Variation of Counting Sensitivity With Depth in Tissue for a Plutonium Source and a Solid State Detector

differentiate multiple sources at various depths and the amount and distribution of surface contamination. None of the present detectors provides the desired degree of information; however, the advances made with solid state detectors permit the addition of more information to that presently available.

The NaI(Tl) scintillation detector will probably remain the wound counting unit of choice for some time because of its adequate information and its low cost. For a typical NaI(Tl) unit, an MDA of 0.1 nCi⁽⁴⁾ is possible whereas we have seen that an MDA of 0.25 nCi results from using the lithium-drifted silicon detector. A surface-contoured diode held at approximately 2.4 cm from the wound can detect an MDA of about 40 nCi. This 2.4 cm represents about the same distance as required by the lithium-drifted silicon detector to the source; however, the surface-contoured diode can be placed much closer to the wound, thus compensating for its low intrinsic efficiency.

REFERENCES

1. K. L. Swinth. "Surface Contoured Diode Applications," Pacific Northwest Laboratory Annual Report for 1967 in the Physics Sciences, Vol. II, Part 1: Instrumentation, BNWL-715, p. 41. Pacific Northwest Laboratory, Richland, Washington. 1968.
2. K. L. Swinth. "Dependence of Plutonium X-ray Counting on Isotopic Composition," presented at 18th Annual Health Physics Society Meeting, Washington, D.C. June 1967.
3. H. E. Palmer, N. A. Wogman, and J. S. Cooper. "The Determination of the Depth and Amount of ²³⁹Pu in Wounds with Si(Li) Detectors," Proc. of the Symposium on Diagnosis and Treatment of Deposited Radionuclides, Richland, Washington, May 1967, pp. 164-170. Excerpta Medica Foundation, Amsterdam. June 1968.
4. W. C. Roesch and J. W. Basm. "Detection of Plutonium in Wounds," Proc. Intern. Conf. on Peaceful Uses of Atomic Energy, 2nd Conf., Geneva, 1958, 23, p. 142. 1959

0012019

SUPPRESSION OF PARTIAL ENERGY DEPOSITION EVENTS IN A SOLID STATE DETECTOR

The suppression of the background continuum in solid-state detectors by anticoincidence and/or pulse-shape discrimination aids in the interpretation of spectra and enhances the peak to Compton ratio. Studies were performed with both ^{137}Cs and ^{59}Fe sources. For the ^{59}Fe source, an average reduction of 85% in the continuum resulted using a planar diode 110 mm^2 by 2.4 mm deep in an anticoincidence annulus of NaI(Tl). Both the distribution and the number of events rejected vary with the amplifier shaping time constants.

Investigator:
K. L. Swinth

INTRODUCTION

The masking of weak, low energy gamma rays by the background continuum resulting from higher energy gamma rays, seriously limits the usefulness of solid state detectors in gamma ray spectroscopy. Reduction of the continuum from high energy gamma rays aids in the identification and quantification of isotopes with weak, low energy gamma emissions. Most of this continuum results from Compton interactions in the detectors themselves and in nearby materials. Recent work suggests that these interactions occur in the dead layers of solid state detectors.^(1,2)

The interaction of gamma rays and their secondary electrons in the dead layers (poorly compensated regions) of the diode results in pulses with a slow rise-time component.⁽³⁾ Trapping and carrier recom-

bination, enhanced in the dead layer due to a weak collecting field, cause a loss of collected charge and a slow rise-time pulse. Because of this loss of collected charge, pulses of reduced amplitude result which are not proportional to the energy deposited by the primary event, thus degrading the energy spectrum. Standard pulse-shape discrimination techniques can reject pulses with such slow rise-time components.

This paper describes the overall results obtained using both pulse-shape discrimination and anticoincidence counting with a solid-state detector. The following paper, "Development of Pulse-Shape Discrimination Circuitry for Suppression of Partial Energy Deposition Events", by N. C. Hoitink and L. D. Philipp, describes circuitry developed for these experiments.

0012020

DISCUSSIONDetectors

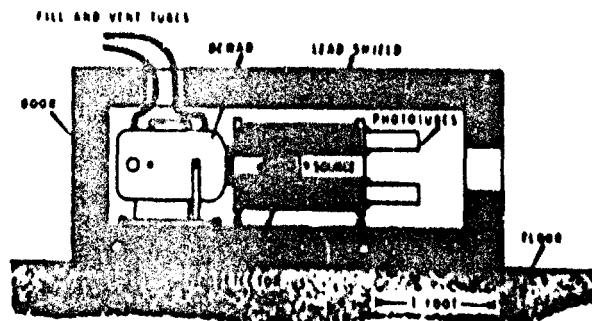
The small solid state detector used in these studies has an area of 110 mm^2 and a depletion depth of 2.4 millimeters. At the 1.33 MeV ^{60}Co line, this detector achieves a resolution of 5.0 keV FWHM with a peak to Compton ratio of 2:1. The detector operates with an applied electric field of 950 V/cm; has a diffused region of about 0.3 mm and an undepleted region of about 1 mm. It mounts in a satellite dewar on a 17.8 cm (7 in.) copper cold finger. A 5.72 cm (2 1/4 in.) outside diameter vacuum containment shroud of 0.483 mm (0.019 in.) aluminum covers the detector which is 2 cm from the end.

The anticoincidence detector comprises a 20.3 cm (8 in.) diameter by 30.5 cm (12 in.) long sodium iodide annulus with a 6.35 cm (2 1/2 in.) inside diameter tunnel with aluminum walls 0.483 mm (0.019 in.) thick. The annulus splits lengthwise along its axis to form optically isolated halves each viewed by three RCA 8053 photomultiplier tubes with magnetic shields. Somewhat similar to that described by R. L. Auble, et al., the annulus was selected because of its versatility for general purpose counting.⁽⁴⁾ Although it can be used as a pair spectrometer, for high

level counting with an external source, or for general coincidence counting, this paper discusses only its use as an anticoincidence detector with an interior source. The resolution of this detector for a centrally located source of cesium is 11% FWHM. Figure 1 illustrates the anticoincidence annulus and the satellite dewar showing their relative positions. The dewar and the anticoincidence detector mount horizontally inside a 10.2 cm (4 in.) thick lead shield with inside dimensions of 91.4 cm (3 ft) long, 30.5 cm (1 ft) high and 40.6 cm (16 in.) wide. Both the dewar and the anticoincidence detector are track mounted so that they may be easily moved in and out of the shield.

Circuitry

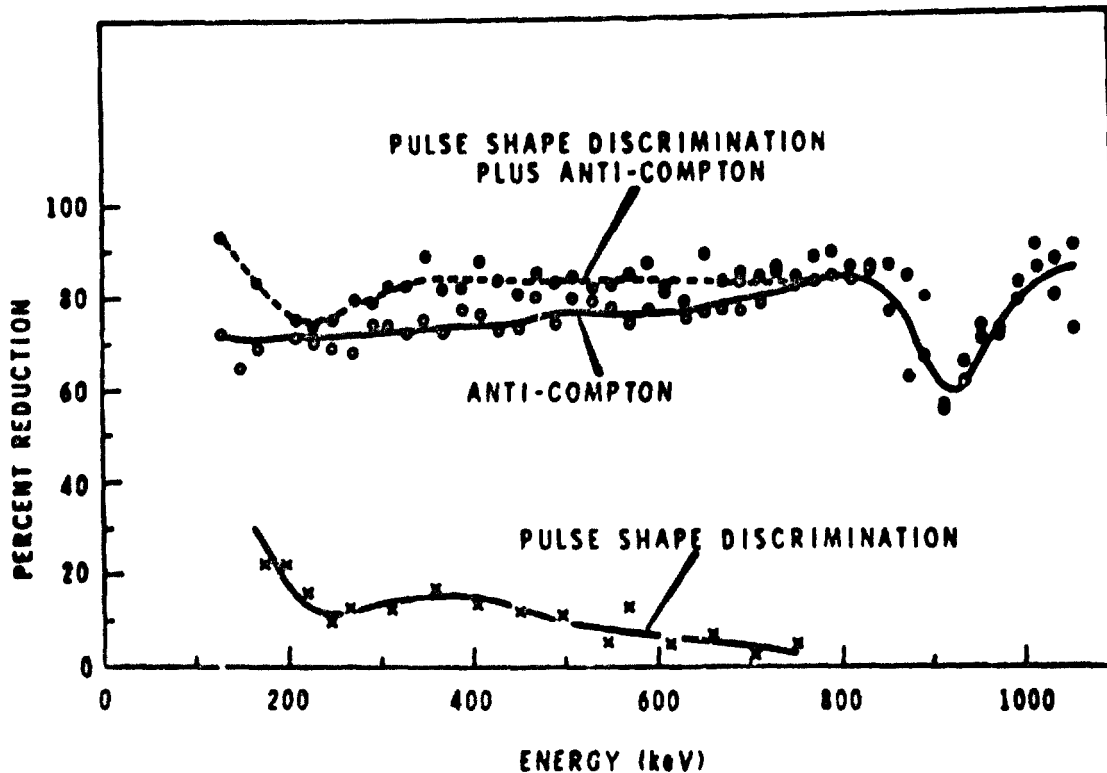
As mentioned previously, discussion of the pulse shape discrimination circuitry is presented by



Neg 0680788-7

**FIGURE 1 - Relative Positions of
Solid State Detector and
Anticoincidence Detector**

0012021



Neg 0680728-3

FIGURE 3 - Reduction in the Continuum From ^{59}Fe With Pulse Shape Discrimination and Anticoincidence Counting

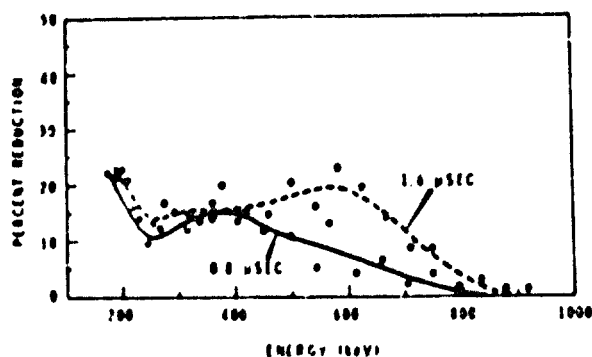
low energies results from the back-scatter peak while a similar dip at high energies occurs in the region of the Compton edge where the anticoincidence shield loses its effectiveness. In general, the reductions from the anticoincidence shield and the pulse shape discrimination are not quite additive. Figure 3 indicates that for ^{59}Fe primary photons, pulse shape discrimination loses importance above approximately 700 keV.

Similar results were obtained for a ^{137}Cs source. Average reductions of 8%, 82% and 87% were obtained in the energy region from 100

keV to 450 keV using pulse shape discrimination, the anticoincidence mode, and the combination mode, respectively. Pulse shape discrimination does not appear effective above 350 keV in this case. In the energy range of greatest effectiveness (100-350 keV) the average reduction using pulse-shape discrimination is 11%.

One would also expect the pulse shape discrimination technique to be dependent upon the amplifier shaping time constants. With longer time constants the ballistic deficit decreases for a pulse with a slow rise time component resulting in the movement of the spectrum of slow

0012023



Neg 0680722-4

FIGURE 4 - Effect of Amplifier Time Constants on Pulse Shape Discrimination Operation

rise time pulses toward higher energies. (3) Figure 4 demonstrates results obtained in the pulse-shape discrimination mode using two different amplifier time constants and a ^{60}Co source. The lower curve results from equal integration and differentiation time constants of 0.8 μsec while 1.6 μsec time constants were used to obtain the upper curve. The average reduction using the 0.8 μsec time constant is 11.5%, while that for the 1.6 μsec time constant is 14.5%. Similarly, time constants of 0.4 μsec and 3.2 μsec resulted in reductions of 10.5% and 16.4%, respectively.

Tests were also conducted to determine the effect of varying the electric field across the intrinsic region. Significant variations in the percent reduction by pulse-shape discrimination were not observed when the field was varied in steps

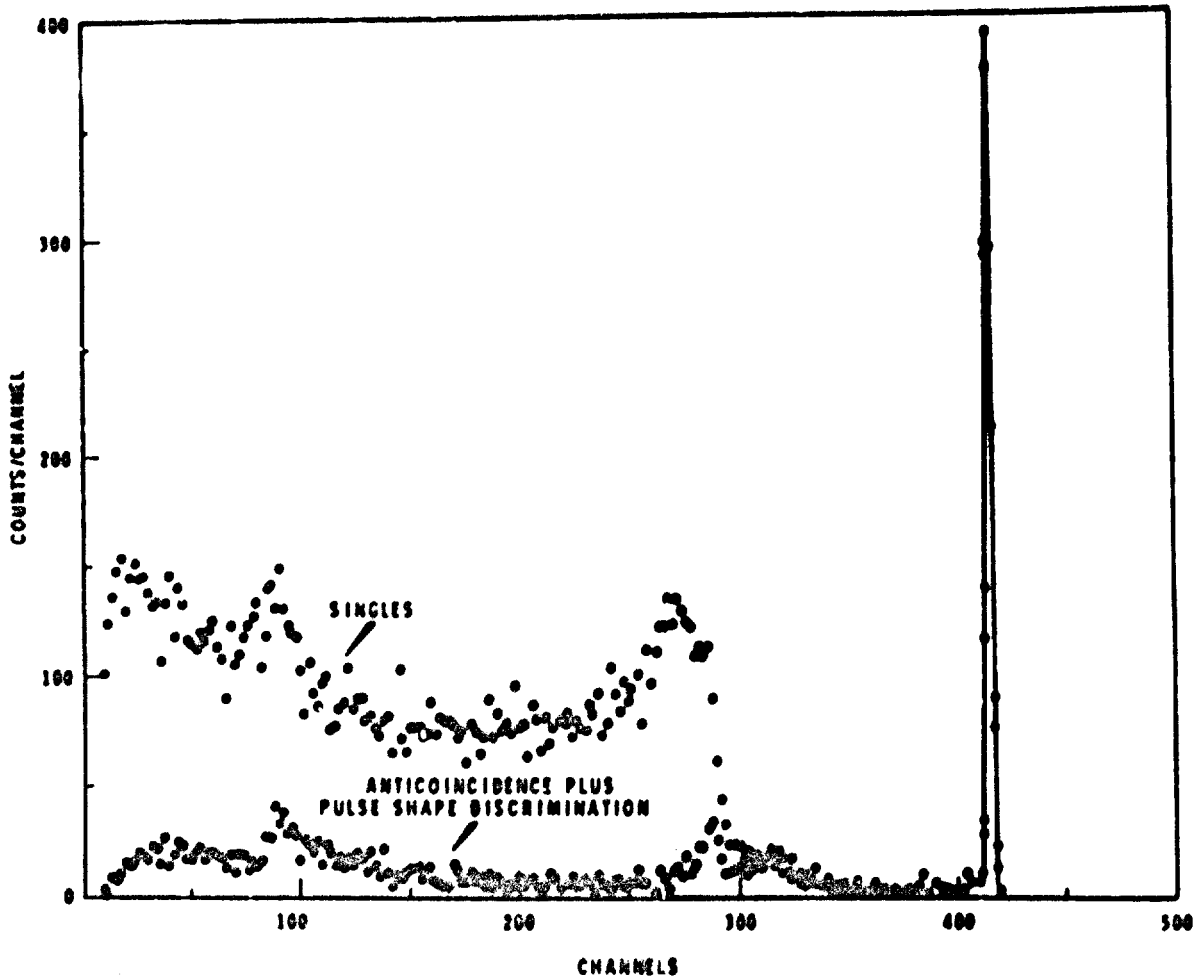
from 500 V/cm to 1250 V/cm.

Figure 5 shows an energy spectrum of ^{137}Cs without correction and one with both pulse shape discrimination and anticoincidence modes of operation.

The value of these methods in reducing the continuum is obvious from this figure. A spectrum for anticoincidence is not included since it tends to merge with the combination mode at these count rates.

CONCLUSIONS

In general, anticoincidence counting provided an average reduction of 80% in the continuum from high energy gamma rays. In the energy region from 100 keV to 70% of the photopeak energy, a typical reduction in the continuum of 10% was obtained using pulse-shape discrimination. Above 70% of the photopeak energy, pulse shape discrimination was not effective. The two methods of continuum reduction are not additive on a one to one basis. Apparently some of the slow rise time events result from gamma rays which also interact in the anticoincidence detector. Slightly over one-half the reduction by pulse-shape discrimination adds to the reduction by anticoincidence. Of course, pulse-shape discrimination is more impres-



Neg 0880745-1

FIGURE 5 - ^{137}Cs Spectrum Showing Reduction in the Continuum with Pulse Shape Discrimination Plus Anticoincidence Counting

sive when compared with a spectrum already reduced by anticoincidence. In the case of ^{137}Cs , the anticoincidence spectrum is reduced by an average of 30% with pulse-shape discrimination. Over this same energy region (100 keV to 450 keV) an average reduction of only 8% is obtained when compared to the not-in-coincidence continuum.

We obtained less reduction than that of up to 25% to 30% reported by other investigators although values of over 20% were obtained in the lowest energy portions of the spectrum. ^(1,7) Our results and the work of others indicate that pulse shape discrimination is effective during investigations covering a wide range of energies.

0012025

REFERENCES

1. U. Tamm, W. Michealis and P. Cousseu. "A Pulse Shape Discrimination Circuit for Lithium-Drifted Germanium Diodes", Nucl. Instr. and Meth., Vol. 48, pp. 301-305. 1967.
2. M. G. Strauss and R. N. Larsen. "Pulse Height Defect Due to Electron Interaction in the Dead Layers of Ge(Li) γ -Ray Detectors", Nucl. Instr. and Meth., Vol. 56, pp. 80-93. 1967.
3. M. G. Strauss, R. N. Larsen and L. L. Sifter. "Pulse Shape Distributions From Gamma-Rays In Lithium-Drifted Germanium Detectors", IEEE Trans. Nucl. Sci., Vol. NS-13, p. 285. June 1966.
4. R. L. Auble, D. B. Barry, G. Berzins, L. M. Bayer, R. C. Etherton, W. H. Kelley and W. C. Morris. "Coincidence-Anticoincidence Gamma-Ray Spectroscopy with NaI(Tl) Split Annulus and a Ge(Li) Detector", Nucl. Instr. and Meth., Vol. 51, pp. 61-71. 1967.
5. T. K. Alexander and F. S. Goulding. "An Amplitude Insensitive System That Distinguishes Pulses of Different Shapes", Nucl. Instr. and Meth., Vol. 13, pp. 244-246. 1961.
6. T. K. Alexander, J. D. Pearson, A. E. Litherland and C. Broude. "Pulse-Shape Discrimination on The Gamma-Ray Pulses From $F^{19}(d, n\gamma)Ne^{20}$ Observed With a Lithium-Drifted Germanium Gamma-Ray Spectrometer", Phys. Rev. Ltrs., Vol. 13, pp. 86-88. July 1964.

DEVELOPMENT OF PULSE SHAPE DISCRIMINATION CIRCUITRY FOR COMPTON SUPPRESSIONAPPLICATIONS

The proper use of pulse shape discrimination techniques aids suppression of the background continuum in spectra obtained using solid-state detectors. This suppression improves the interpretation of spectra and enhances the peak-to-Compton ratio. This paper describes development of pulse shape discrimination circuitry for use with or without anticoincidence techniques to investigate possible improvements in Compton suppression

Investigators:
N. C. Hoitink
L. D. Philipp
Technical Assistance:
J. Harlow

INTRODUCTION

The interaction of gamma-rays, or their secondary electrons in the dead layers (poorly compensated re-

gions) of solid state detectors, results in pulses with a slow rise-time component.⁽¹⁾ Trapping and carrier recombination, enhanced in the dead layer due to a weak collec-

ting field, cause a loss of collected charge and a slow rise-time pulse. Because of this loss of collected charge, pulses of reduced amplitude (not proportional to the energy deposited by the primary event) result, thus degrading the energy spectrum. Standard pulse-shape discrimination techniques can reject pulses with such slow rise-time components.

The circuits described in this paper resulted from developments related to a need in a solid state detector counting system for reducing the continuum of the energy spectrum from gamma-rays in the energy range from 100 keV to 1.5 MeV. The paper "Suppression of Partial Energy Deposition Events in a Solid State Detector" by K. L. Swinth, contained elsewhere in this report, describes the overall results of the investigation, including the improvements attributable to the pulse shape discrimination circuits described herein.

DISCUSSION

Of the various methods of pulse-shape discrimination researched and found suitable for use in eliminating the slow time constant pulses, two methods proved worthy of investigation. The method described by Alexander and Couling⁽²⁾ utilizing

the shift in baseline crossover did not adequately cover the energy region of interest. Discriminator "walk" and difficulty in proper system adjustment were the limiting factors. To meet the requirements of the current experiments, we developed a circuit after the method of U. Tamm et al.⁽³⁾

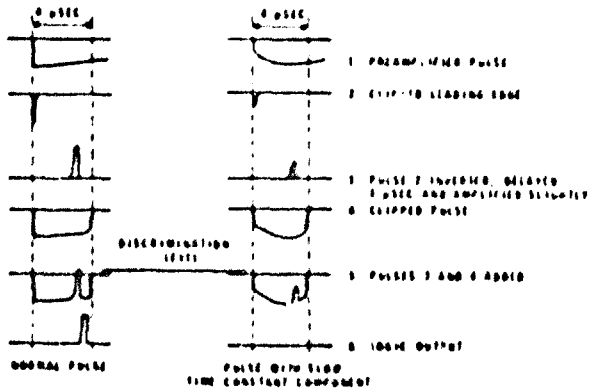
Normal pulses from full energy events in the intrinsic region exhibit typical rise times on the order of 10 nsec. This means that good pulses will exhibit a rise time limited by the preamplifier, typically on the order of 50 nsec, and a decay time also characteristic of the preamplifier, usually 50 to 100 μ sec. Pulses with a slow rise-time component result from interactions in the dead layers of the diode detector. These pulses will not reach their maximum height (all of the charge will not have been collected) until after a few microseconds. Figure 1 illustrates both types of pulse. Now, if one compares the leading portion of each pulse with the pulse at some later time, it can be determined if the pulse has a slow rise-time component. This method should be independent of pulse height. After clipping a fraction of a microsecond from the leading edge of the pulse, inverting it and adding it back onto the pulse following a

suitable delay (typically 3 μ sec), a normal pulse will cross the baseline but one which exhibits a slow rise-time component will not, as illustrated in Figure 1.

The block diagram of Figure 2 and the complete circuit diagram of Figure 3 represent circuitry developed at PNL utilizing the described method. The pulse from the preamplifier has a rise time of 60 nsec with a decay time of 44 μ sec. After initial amplification, one portion of the circuit clips the pulse to a 4 μ sec width, while in the other part of the circuit the front edge is clipped to 0.2 μ sec and delayed 3 μ sec. The resulting pulses then add to the original pulse in a summing amplifier, after which the gain on the 0.2 μ sec pulse can be adjusted so the pulse just crosses the baseline and triggers a discriminator.

The integrated circuit comparator used as the discriminator has a discrimination level about 5 mV above the baseline and when triggered, drives a monostable circuit resulting in a logic signal.

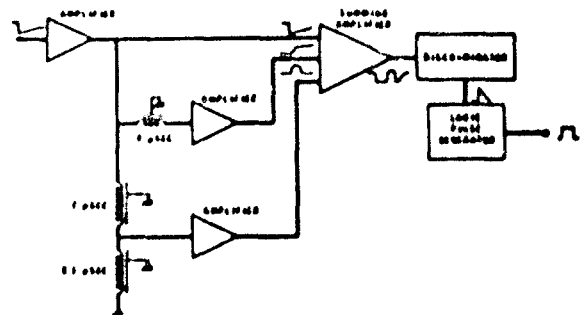
Calibration with a pulse generator permits proper gain adjustment of the 0.2 μ sec channel for acceptance of all test pulses above a selected energy level. Below this energy, pulse height fluctuations of the 0.2 μ sec pulse caused by preamplifier noise result in improper operation of the circuit. Generally, circuit adjustments permitted proper operation for pulses over 100 keV, and the circuit provides a dynamic range of 50 to 1. In practice, a shift of less than 5 mV in the desired discrimination level results over a dynamic range of 10 to 1. This shift, unimportant over the



Neg 0680722-1

FIGURE 1 - Illustration of Pulse Relationships for the Pulse Discrimination Circuit

0012028



Neg 0680722-6

FIGURE 2 - Block Diagram of the Pulse Discrimination Circuit

range of interest, occurs because of the gain added to the 0.2 μ sec pulse to eliminate noise fluctuations. Comparison of detector pulses on an oscilloscope shows apparent rejection of 100% of pulses with a slow rise-time component.

RESULTS

As mentioned, the results obtained using the described circuits are detailed in the paper by K. L. Swinth. The complete investigation included the use of both pulse shape discrimination and anticoincidence techniques.

Using a ^{59}Fe source, the average reduction in the Compton distribution using just the pulse shape discrimination proved to be 13.5% in the range from 100 keV to 550 keV and 6% in the range from 550 keV to 800 keV. Spectra obtained using a ^{137}Cs source reveal reductions in the Compton distribution averaging 11% over the range of 100 to 350 keV. The pulse shape discrimination technique does not appear to be effective

above 700 keV (using the ^{59}Fe source) or above 350 keV (using the ^{137}Cs source).

Use of the single sweep feature of an oscilloscope (several observations) afforded a comparison of the observed pulse shape and the ability of the circuit to discriminate between normal pulses and those with a slow rise-time component. For the sample observed, the correlation proved to be 100%.

REFERENCES

1. M. G. Strauss, R. N. Larsen and L. L. Sifter. "Pulse Shape Distributions From Gamma-Rays in Lithium-Drifted Germanium Detectors", IEEE Trans. Nuc. Sci., Vol. NS-13, p. 285. June 1966.
2. T. K. Alexander and F. S. Goulding. "An Amplitude Insensitive System That Distinguishes Pulses of Different Shapes", Nucl. Instr. and Meth., Vol. 13, pp. 244-246. 1961.
3. U. Tamm, W. Michaelis and P. Cousieu. "A Pulse Shape Discrimination Circuit for Lithium-Drifted Germanium Diodes", Nucl. Instr. and Meth., Vol. 48, pp. 301-305. 1967.

4)

FEASIBILITY OF USING CROSS-CORRELATION TECHNIQUES TO
DETERMINE IN VIVO RADIONUCLIDE LOCATIONS

Evaluation of the theoretical and technical feasibility of using a proposed cross-correlation system to determine in vivo location and intensity of radionuclides indicated that the specific method used would not be able to locate distributed sources with the required accuracy. The paper describes both the theoretical and experimental considerations.

Investigator:
T. H. Morton

INTRODUCTION

A proposed cross-correlation system for determination of radionuclide location and intensity was evaluated for its theoretical and technical feasibility. It was anticipated that the proposed location system would be useful for radionuclides exhibiting negligible self-absorption and could lead to the development of automatically produced plots of organ-tissue uptake patterns, iso-intensity plots or time-space patterns.

DISCUSSION

In the initial study, a 10 μ Ci point source of ^{137}Cs was positioned in a water phantom which simulated the effects of tissue on gamma-rays. The phantom was then scanned circumferentially in the source plane by a detector whose collimator provided a serial width of the examined sector

throughout the scan (see Figure 1). Successively placing the radiation source within a position matrix in the phantom simulated various locations of translocated radionuclides. In the first study, twelve circumferential scans were made, each with the point source in a different known position within the phantom as shown in Figure 2.

Data from these scans produced twelve curves, typified by the examples of Figure 3. These curves permitted evaluation of cross-correlation techniques which might be used to locate an unknown point source from its curve of intensity versus θ . The area normalized cross-correlation function, $\rho_r(\theta_1)$, gives the probability that a point source of unknown location is positioned at a particular angle θ_1 and radius r_n , where θ_1 differs from θ by from 0° to 360° and r is the radial location from the center of the phantom. In

0012031

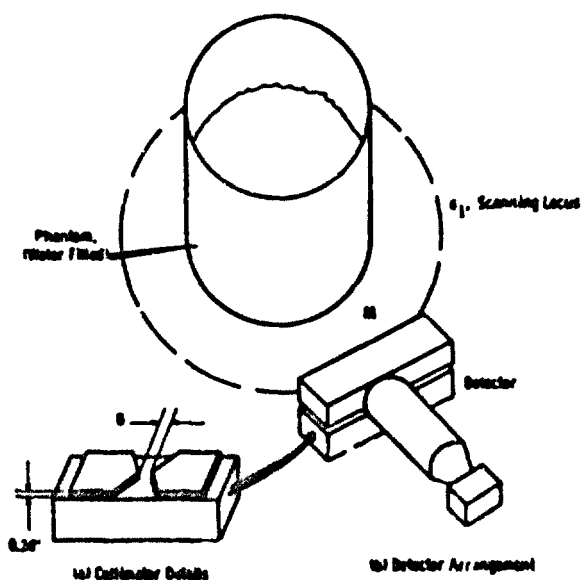


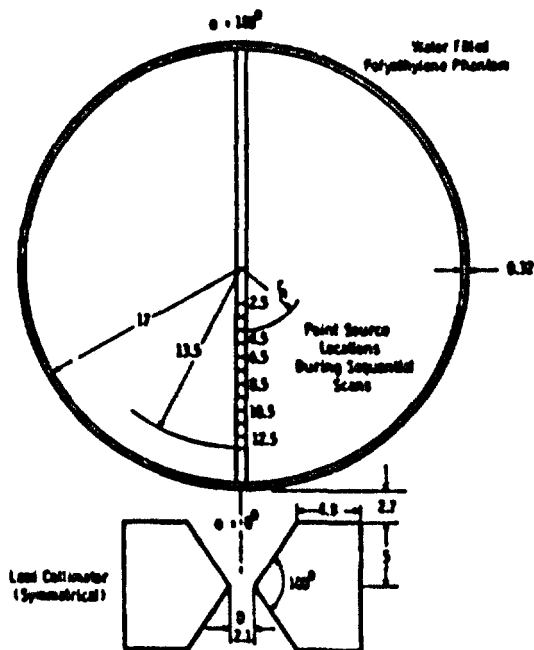
FIGURE 1 - Scanning Configuration

this study r_n varies from r_1 (2.5cm) to r_{12} (13.5 cm) and $\rho_1(\theta_1)$ is given by

$$\rho_1(\theta_1) = \frac{\int k_1(\theta - \theta_1) u(\theta) d\theta}{\sqrt{\int k_1^2(\theta) u^2(\theta) d\theta}}$$

where $k_1(\theta)$ is the intensity versus θ curve for a point source located at a known location (r_1, θ_0) and $u(\theta)$ is the curve of radiation intensity versus θ for the ^{137}Cs point source having an unknown location. Because $u(\theta)$, in this work, is located at $\theta = 0$, when $k(\theta)$ and $u(\theta)$ perfectly correlate, $\rho(\theta_1)$ will equal one at $\theta_1 = 0$ and will be less than one for θ_1 greater than zero but less than 360° . For curves of $k(\theta)$ different from $u(\theta)$, $\rho(\theta_1)$ will be less than one at $\theta_1 = 0$. However,

0012032



Note: Measurements are in Centimeters

FIGURE 2 - Source Location and Collimator Details

analog computer analysis of data obtained using the first collimator, Figure 2, indicates that when $k(\theta) = u(\theta)$, as θ_1 changes from 0° , $\rho(\theta_1)$ decreases very slowly. These curves are shown in Figure 4. Furthermore, at $\theta_1 = 0^\circ$, $\rho(0^\circ)$ decreases from unity very slowly for $k(\theta)$ obtained from radionuclide point sources located at radial positions different from those of $u(\theta)$ as shown in Figure 5. This poor system resolution results from the slow variation of $\rho(\theta_1)$ with radial and angular location of the calibration point source. The slow variation of $\rho(\theta_1)$ is caused by the great simplicity of the curves $k_1(\theta)$ to $k_{12}(\theta)$ and their

relative similarity.

Experimental results of efforts to improve resolution by varying the collimator aperture, D , indicate that the intensity-displacement curves remain similar regardless of aperture opening or radial location of the source in the phantom. Further study indicated that perhaps certain detector collimator configurations, Figure 6 for example, could be designed which would increase the complexity of these $k(\theta)$ curves to improve the cross-correlation system resolution. The variables considered in analysis of the collimator include the collimator material and configuration, the detector scanning locus, and the length of the collimator holes.

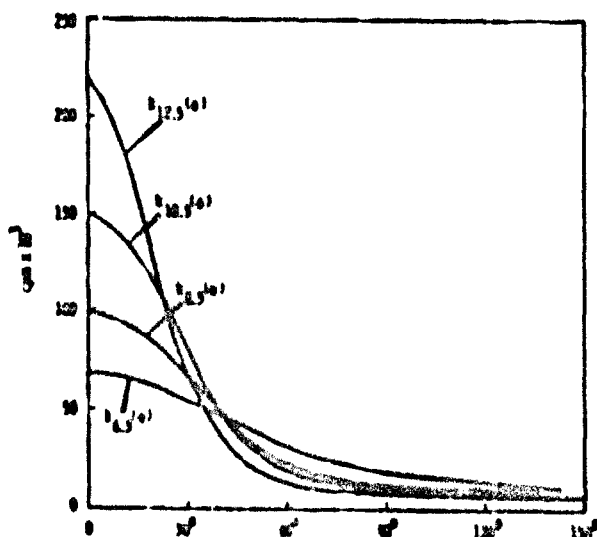


FIGURE 3 - Typical Point Source Scans, $k_p(\theta)$

0012033

In a theoretical study, two examples were used to investigate collimator variables and their effects on cross-correlation functions. The first example concerned the point source cross-correlation of a curve $k_{T_n}(\theta_n)$ with a similar curve for $k_{T_n}(\theta_n)$. Even with more complex collimator configurations, this example demonstrated that, with the point sources located as described, the cross-correlation system erroneously indicates the radial location of the radionuclide.

The second model investigated the cross-correlation of the curve $k_{T_n}(\theta_n)$ with the curve $k_{T_m}(\theta_m)$. In this case, point source position errors result from two causes. First, even if the collimator aperture

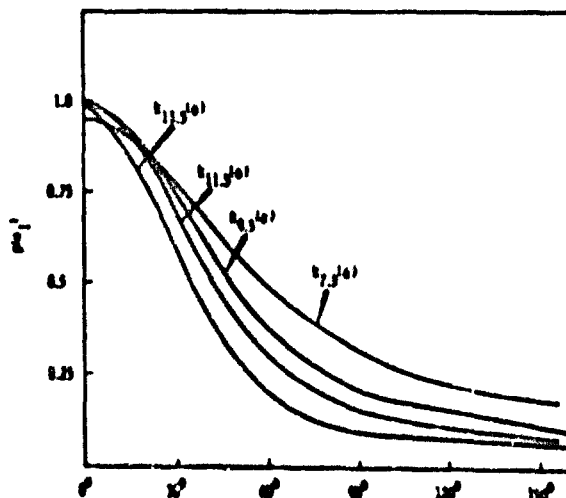


FIGURE 4 - Cross Correlation Functions for $u(\theta) = k_{11.5}(\theta)$

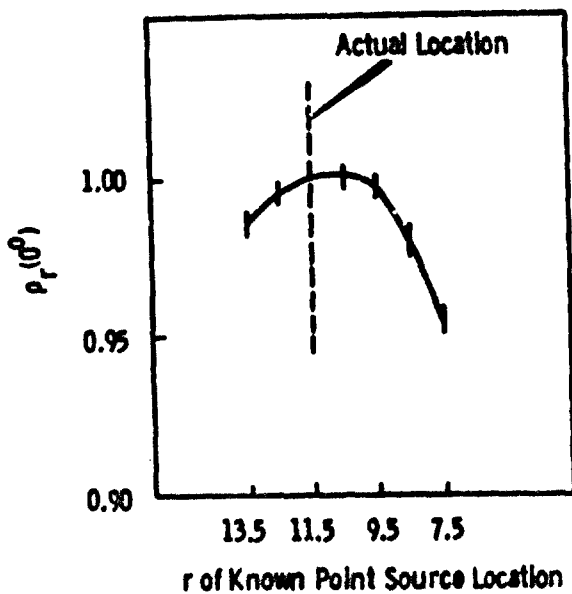


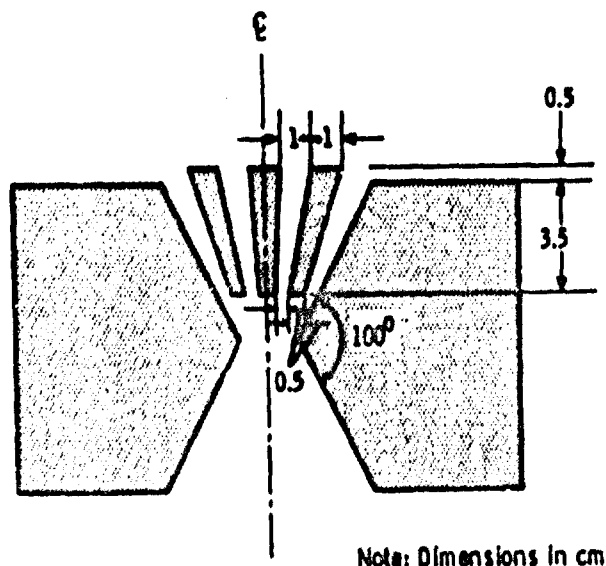
FIGURE 5 - Area Normalized Cross Correlation With 0° Phase Shift For ^{137}Cs Point Sources at $r = 11.5$ cm
angles are optimized and possibly randomized, they must have some finite value and some amount of false location of the point source will result because of the properties of the correlation operation. Also, error will result because perfect collimation of the gamma-rays is not possible.

In vivo studies would be further complicated due to the presence of distributed instead of point sources which result from deposition of specific radionuclides in preferential organs. Other variables contributing to the overall inaccurate location of sources using the cross-correlation techniques include subject movement (during long counting

times), inhomogeneities of gamma-ray absorption properties, and scattering. The cross-correlation system's usefulness is determined by the accuracy desired in the location of radionuclides, reasonable counting times, and the allowable source strength within the subject.

CONCLUSIONS

The resulting high error probability in accurately locating radionuclide depositions in the simulated biological system by cross-correlation techniques suggests that further experimental effort include more sophisticated collimator configurations as well as consideration of lower energy isotopes.



Note: Dimensions in cm

FIGURE 6 - Lead Collimator Configuration

0012034

MINIATURE IMPLANTABLE HIGH VOLTAGE SUPPLY

The described compact voltage supply for miniature G.M. tubes will permit the acquisition and telemetry of radionuclide uptake information and conventional physiological parametric data from experimental animals. The unit operates from a 2.7 V battery, requires 0.5 mA of current, and measures 1.5 cm diam by 2.3 cm long.

Investigators:
E. M. Sheen
R. L. Wilbur
Technical Assistance:
R. M. Ferdinand

INTRODUCTION

For biotelemetry of radionuclide uptake information, the Geiger-Mueller tube offers the important advantage of providing large output signal pulses that require little amplification. Miniature G.M. tubes suitable for implantation require several hundred volts to bias the tube in the proper plateau region, but output average current from the bias source for exposure rates anticipated in experimental investigations typically equates to less than 50 nA. The plateau region may be as low as 10% of the center voltage, thus requiring regulation within a few percent.

A compact voltage supply developed by Dilworth et al.⁽¹⁾ provided the necessary potential and current requirements for miniature G.M. tubes operating to very high exposure rates. This bias source operated from a 4 V mercury battery and utilized feedback to increase both

frequency and output of a transistor blocking oscillator with exposure rate. A voltage quadrupler rectified the output pulses and provided the necessary output potential. The experiments reported here focus on necessary design/development and fabrication changes in the basic Dilworth circuit to minimize volume, operate from a 2.7 V battery (compatible with a commercial pulse-width modulated implantable telemetry unit) and be implantable.

DISCUSSION

Figure 1 shows the circuit diagram of the miniature blocking oscillator high voltage supply. Prior to generating a pulse, the transistor does not conduct, and the transformer presents an equivalent circuit to the collector in which the mutual inductance dominates. Current from R1 begins to turn on the transistor and the collector voltage e_1 becomes negative. Regeneration occurs because a positive voltage

0012035

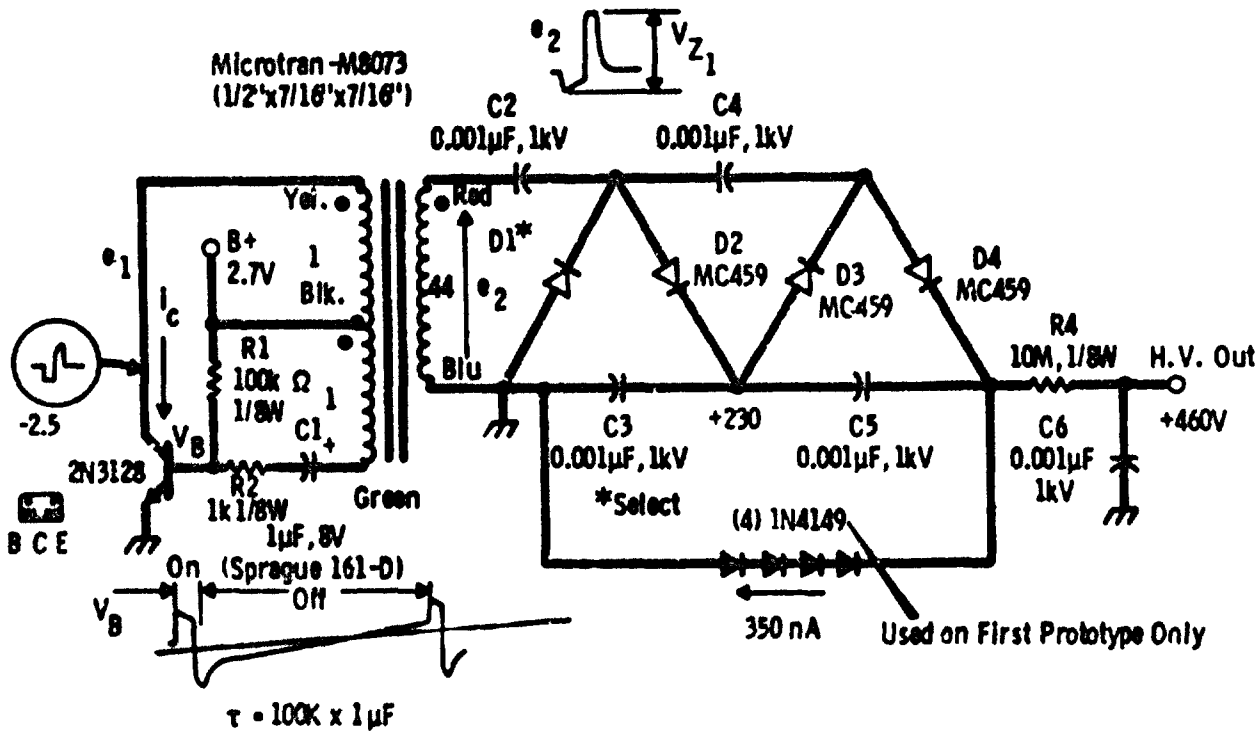


FIGURE 1 - Circuit Diagram

(-e₁) from the feedback winding increases base current as the collector voltage drops. When the transistor saturates, collector current increases nearly linearly at a rate $\frac{di_c}{dt} = \frac{2.7 - V_{set}}{M}$, where M is the transformer mutual inductance. At this same time (following transistor saturation), the base current decreases with a time constant equal to (R2)(C1), approximately 1 msec. The transistor collector voltage starts positive again with $i_c = \beta i_b$ and the feedback voltage regeneratively turns off the transistor.

After the pulse occurs, the base voltage remains negative (because of the voltage developed across C1 dur-

ing the ON state) and slowly returns with an (R1)(C1) time constant. Initially during the ON period, the output voltage, e₂, equals the turns ratio (44:1) times e₁, or approximately -100 V, and D1 conducts to charge C2. The collapsing magnetic field of the transformer generates a large positive voltage and places charge on C3 through D2, back-biasing D1. If the reverse voltage avalanche point of D1 occurs at a voltage V_{Z1}, the maximum voltage across C3 limits at V_{Z1}. This limiting action serves as a basis of regulation because C4 ac-couples a voltage V_{Z1} (peak-to-peak) through the second diode pump, thus again placing V_{Z1}

0012036

across C5 to give an output voltage of $2V_{Z1}$. This process assumes a negligibly small charge moves from C3 and C5 through the output load between pulses. In the original circuit, specially selected 1N459 general purpose silicon signal diodes (200 PIV rated) served the voltage regulating function.

Microminiature diodes, such as provided by Microsemiconductor Corporation, offered promise in reducing the total supply volume. Unfortunately, selection from twenty-four MC459 and MC458 diodes with minimum 200 PIV and 150 PIV ratings respectively, yielded only one unit with V_{Z1} near 200 V. Most of these devices avalanched at potentials greatly in excess of the minimum value (1 kV typically). For the prototype implantable unit, a value of 100 k Ω for R1 gave the desired 475 Vdc output, compatible with an EON Type 5307 G.M. tube (0.097 in. diam x 0.4 in. long, halogen quench), and 140 nA through the 1N4149 series. This experience indicates the probable need to purchase selected units (with desired avalanche point) directly from the diode vendor, rather than attempting sorting from stock. The final flux value, proportional to the collector current, depends on transistor β . Resistor R1 should, therefore, be selected for a partic-

ular 2N3128 to give the desired output current capability. The four 1N4149 diodes connected in series gave a voltage change of 465 Vdc to 480 Vdc for currents from 135 nA to 520 nA. The nominal current obtained for the prototype measured 350 nA and a load current of 130 nA resulted in a 5 volt high voltage drop from 475 V (no load) at 130°F. Voltage variation due to temperature rise from 72° F to 130° F was less than 2 volts.

The micro-transistor, 2N3128, further reduced total volume. The transformer and capacitors remain dominantly large. However, incorporation of unencapsulated ceramic capacitors (such as Eire Corp. 8000-008 "Monoblock" 0.002 μ F, 1 kV), or removal of the phenolic coating and large connecting wires from standard ceramic capacitors, reduced the capacitor volume to one half. Miniature low voltage tantalum capacitors are readily available.

The experimental prototype operates from a 2.7 V battery, requires only 0.4 mA of quiescent current, and provides sufficient bias current to operate the G.M. tube at 5,000 cpm. Assuming further tests prove satisfactory and following application of medical grade coating, the unit should be suitable for implantation. The prototype, potted in

0012037

clear epoxy, occupies a volume 1.5 cm diam by 2.3 cm long. A voltage drop of approximately 5% occurred at the 5,000 cpm rate. With no avalanche occurring for D1, the unit provides an open circuit output voltage of approximately 700 V. We anticipate further development work to achieve greater circuit reliability.

REFERENCE

1. R.H. Dilworth and C.T. Borkowski, Personal Radiation Monitor, Oak Ridge National Laboratory, Oct. 1981.

IRRADIATION EFFECTS ON CHARGE-MULTIPLYING DIODE DETECTORS

This article presents the conclusions of a program to define the irradiation effects of ⁶⁰Co on passivated and nonpassivated avalanche diodes biased near breakdown. The annual report for 1987 mentioned the experiments which are described in greater detail in a separate formal report.

Investigator:
N. C. Holtink
Technical Assistance:
J. M. Frame, Jr.

INTRODUCTION

Numerous studies have focused on the radiation effects of semiconductor devices, both transistors and diodes, in many different kinds of radiation fields. However, published information concerning such experiments for avalanche diodes operating in or near breakdown, an area of considerable interest to engineers and scientists, have been scarce. Recent

work with solid state radiation detectors has resulted in a new detection technique^(1,2) in which the multiplication characteristics of avalanche diodes biased within a few percent of breakdown produce charge multiplication within the detector. This effect significantly improves the sensitivity and the signal-to-noise ratio available in such detectors.

The experiments utilized twenty Motorola 1N2846 200 V, 50 W, Zener diodes, where 10 were of the passi-

*Supported in part by general Services Assessment funds.

vation variety. Thus, the obtained data describe the effects of passivation on the radiation-induced surface effects of this particular diode. Experiments also focused on both diode types with the encapsulation removed and with modest vacuum applied to the test assembly. These experiments provide information regarding ambient conditions related to radiation effects, for both passivated and nonpassivated devices. Selection of the 1N2846 diodes was on observations made by A.R. Jones⁽³⁾ in which he indicated the suitability of such diodes for radiation detection.

CONCLUSIONS

The ⁶⁰Co irradiation experiments performed with the passivated and nonpassivated avalanche diodes operating at 5% below breakdown show significant differences in irradiation effects, where total exposures up to 1.4×10^8 R were obtained for both types of diodes. Except for expected gamma-generated currents, the passivated diodes showed little or no change in characteristics throughout the irradiation although failure rate was high. The nonpassivated diodes demonstrated much less predictable performance, especially in the continued current increase throughout the tests. However, no

complete failures occurred.

The differences in the performance of the two types of diodes appeared to be due to surface effects of irradiation. The passivated units demonstrated immunity to changes in environmental conditions, while the nonpassivated diodes evidenced significant effects.

These experiments provided valuable basic information concerning the effects of irradiation, especially with respect to surface effects and to the advantages or disadvantages of passivation. However, a primary result of the investigations concerns the fact that particular passivated diodes can be used with success as radiation detectors for relatively high gamma levels, while the nonpassivated diodes evidence little value for such applications because of the rather large and unpredictable changes in measured current as a function of time in the gamma environment.

Another point of significance centers on the observed recovery characteristics of the two types of diodes. The nonpassivated diodes required reduction of the bias voltage to zero to effect recovery, while the passivated units recovered with the bias applied. Consideration of this situation may influence the application of diodes in critical

0012039

circuits.

The passivated diodes evidenced comparative insensitivity in unencapsulated form to environmental conditions, while the characteristics of the nonpassivated diodes were materially affected by the environment. Thus, for low-energy radiation detector applications where diode encapsulation may not be possible, the passivated units would be a logical choice.

Finally, the obtained experimental evidence points to irradiation surface effects as the cause for differences observed between the passivated and nonpassivated diodes. These effects remain difficult to predict with any degree of certainty but SiO_2 passivation as a surface treatment appears to be effective in reducing the problem to an acceptable level for many applications.

REFERENCES

1. L.D. Philipp and N.C. Hoytink. "Irradiation Effects on Semiconductor Detectors and Components", Pacific Northwest Laboratory Annual Report for 1967 to the USAEC, Division of Biology and Medicine, BNWL-715, Part 1, pp. 15-20. Pacific Northwest Laboratory, Richland, Washington, June 1968.
2. N. C. Hoytink. The Effect of ^{60}Co Irradiation of Passivated and Nonpassivated Avalanche Diodes Biased Near Breakdown, BNWL-788. Pacific Northwest Laboratory, Richland, Washington, Dec. 1968.
3. A. R. Jones. γ -Ray Dosimetry, With p-i-n Junction Counters, MAECL-2252. Atomic Energy of Canada, Chalk River, Ontario, Canada, February 1965.

TRITIUM TARGET SCANNING USING SURFACE-CONTOURED
DIODES: PRELIMINARY RESULTS

Deuteron irradiation of tritium deposited on a titanium-coated, stainless steel target produces neutrons by a ${}^3\text{H}(d,n){}^3\text{He}$ reaction. Repeated use of these targets requires a knowledge of the tritium distribution on the planchets to accurately determine the source geometry for close-in neutron irradiations. The irradiation geometry is critical since the source-to-subject distance is small. Fluctuations in the dose rate were noticed, suggesting the possibility of redistribution of the tritium on the target. Because of the small size of the surface-contoured diodes and the large amount of activity available (approximately 5 Ci of ${}^3\text{H}$ per target) these units seemed to be a likely choice for a scanning detector to explore the tritium distribution in targets. This also gave us an opportunity to get practical operating experience with the surface-contoured diodes.

Investigator:
T. H. Morton
Technical Assistance:
R. P. Gribble

INTRODUCTION

Experiments were performed to evaluate instrumentation used to determine target tritium distribution by detecting the Bremsstrahlung and K X rays from the titanium which had been excited by the tritium β^- particles. The initial experiment evaluated the temperature stability of a low noise detector system which used a surface-contoured diode as a detector and a tunnel diode as a fast charge-to-voltage converter. This surface-contoured diode detector system was described in an earlier report. (1) Because of the relatively

stable count rate in the experimental environment, development of complex electronic temperature compensation circuitry was not undertaken.

The initial experiments required manual scanning and utilized an X-Y manipulator to translate the planchet past the detector. The planchets scanned were obtained from our Van de Graaf laboratory. Figure 1 depicts the geometry involved in the scanning. For these first experiments, the lower collimator hole diameter was 0.094 in. The experimental results indicated a poorly detailed correlation between the planchet burned spot and the scan-

0012041

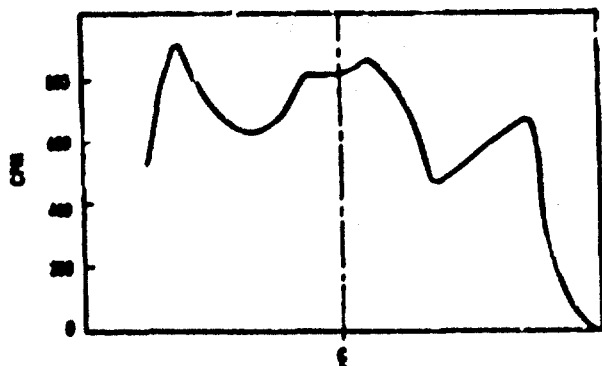


FIGURE 2 - Typical Planchet Scan at Centerline

stainless steel than the titanium surrounding the burned spot. Thus, the radioactivity lost from the

burned spot is small in comparison to that lost by flaking in the surrounding areas. Figure 2 illustrates a typical scan of a target across its centerline.

REFERENCE

1. K. L. Swinth. "Surface-Contoured Diode Investigation," Pacific Northwest Laboratory Annual Report for 1966 to the USAEC-DBM, Vol. II, Part 4, BNWL-481, pp. 40-41, Pacific Northwest Laboratory, Richland, Washington, August 1967.

RADON MONITORING

An alpha scintillation detector system, built to monitor activity levels from 7 nCi/l to 150 nCi/l, monitors radon in an experimental exposure facility.

Investigator:
K. L. Swinth
Technical Assistance:
R. D. Brennan

INTRODUCTION

This report describes a continuous monitor for use in a facility designed for hamster exposure to radon daughters under various experimental conditions. The experimental facility consists of six spherical exposure chambers of 4000

liter (gas, STP) volume. Of the four chambers used for radon exposure, three contain activity levels of about 150 nCi/l while levels in the fourth chamber average about 7nCi/l. One of the three high level (150 nCi/l) chamber systems adds ore dust, another adds diesel fumes, and the third adds room air.

Monitoring of radon and radon daughters is a complex problem due

⁴This activity was funded by the Inhalation Toxicology Section, Biology Department.

to the short half-lives involved and the large number of decay products present. The degree of daughter equilibrium and the presence of unattached daughters are among other factors influencing the isotopes' behavior, biological and physical.

The complexity of the monitoring problem divides it into two facets: first, a monitor continuously evaluates the relative levels of radon in the exposure chambers; secondly, separate systems such as filters, ion chambers, cold charcoal, etc., are used to make periodic measurements to evaluate the degree of daughter equilibrium, absolute activity levels, etc. This report describes only the continuous monitor

which is an alpha scintillator patterned after one described by R. H. Wilson.⁽¹⁾

DISCUSSION

The sampling head for the continuous monitor is simply a box through which a steady flow from the exposure chamber passes. The box has a sensitive volume of 1 liter (gas, STP) and measures 12.5 x 12.5 x 6.3 centimeters deep. On the top of the box is a zinc sulfide (ZnS) scintillator, 10 centimeters by 10 centimeters, attached to a 1 in. thick Lucite light guide optically coupled to a 2 in. photomultiplier tube (RCA 6292).

A diaphragm-type aquarium pump

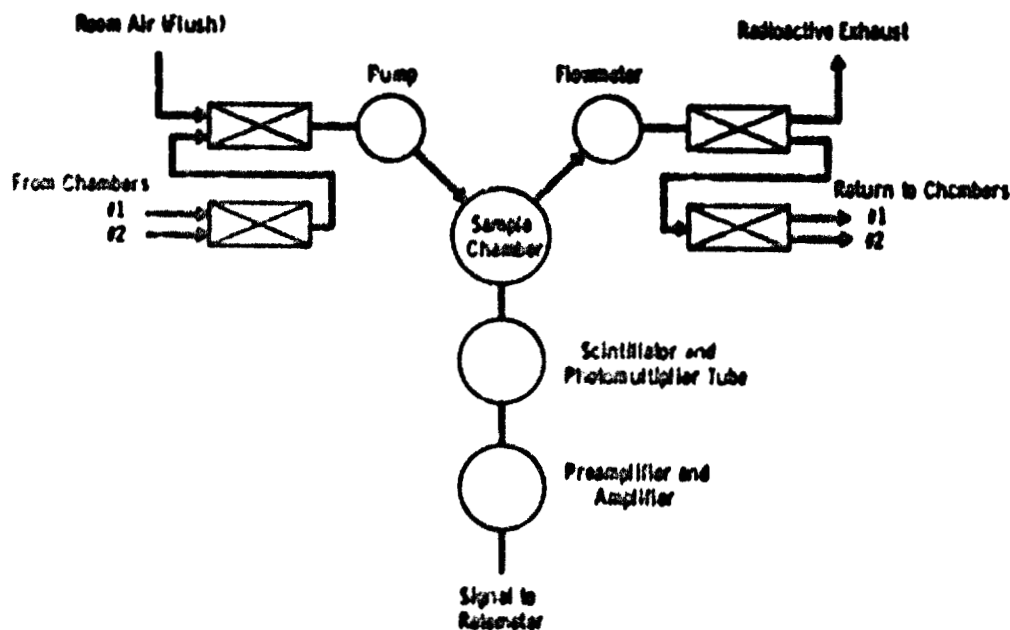
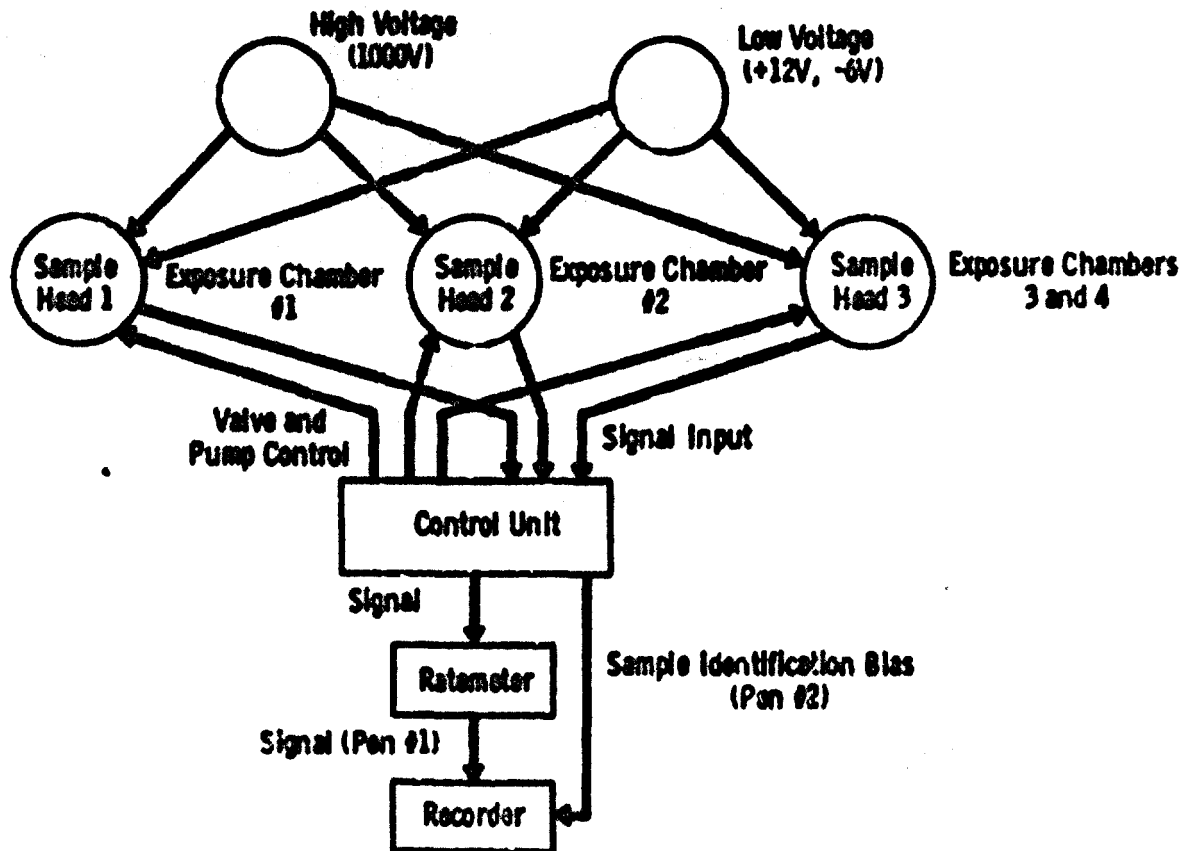


FIGURE 1 - Block Diagram of Typical Sampling Head (Two Chambers)

0012044



**FIGURE 2 - Block Diagram
Continuous Radon Monitor System**

moves air through the box at a flow rate of about 1 liter per minute. A rotameter regulates the flow rate while three-way valves control the input and output of the sampling heads as shown in the block diagram of Figure 1. This scheme permits the sample heads to be flushed with room air.

The entire system comprises three sampling heads, a master control unit, a count-rate meter and a recorder as shown in Figure 2. One of the sampling heads contains two sets of valves so that it can alter-

nately sample two separate chambers. Each of the three photomultiplier tubes has its own preamplifier and amplifier, shown schematically in Figure 3, mounted on its tube base. The output signals from the amplifiers are routed by the control unit to a count-rate meter which drives the strip chart recorder. The control unit contains a timer which sequences the valves, routes the signal and puts a bias level on the second pen of the recorder to identify the sampled chamber. In Figure 4, a simulated recording from the strip

chart, one can see that a portion of the sampling time from each chamber is used to indicate the background in that chamber.

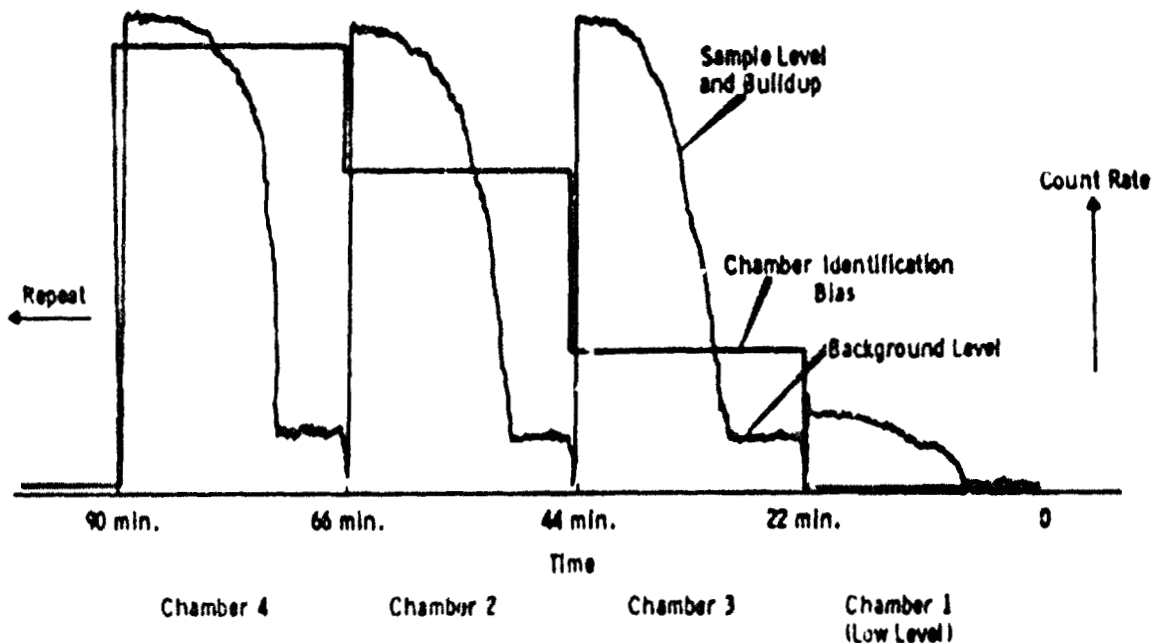
RESULTS

The background in the empty sampling chamber is less than 30 cpm but after radon passes through it at low levels (7 nCi/l), this increases to 150 cpm. The increase apparently results from the attachment of radon daughters to chamber walls and the scintillator surface. Each head samples from an exposure chamber for only 16 minutes out of a full cycle time of 90 minutes. The air entering the sampling head is prefiltered by a membrane filter to take out radon daughters. During sampling the count

rate in the low level sampling head increases to 140 cpm. To avoid range switching on the recorder, the count rates for the high level sampling heads are adjusted to be approximately 9000 cpm. This is done by changing the high voltage on the photomultiplier tube.

CONCLUSIONS

The system is slightly sensitive to electrical transients caused by the opening and closing of the solenoid valves. In general, system operation has been satisfactory and has met its original expectations. In fact, sensitivity has been slightly greater than anticipated. Work continues on a solid state system to measure the radon daughters by



0012047

FIGURE 4 - Simulated Monitor Recording

counting the RaA and RaC' alphas from daughters collected on filter paper.

REFERENCE

1. R. H. Wilson. "Design of a Radium Exposure System," Industrial Hygiene Journal, p. 409. October 1981.

CONTROL SYSTEM FOR IN VIVO NEUTRON ACTIVATION OF SHORT HALF-LIFE NUCLIDES*

This report describes an instrument to automatically correct for half-life decay during in vivo neutron activation experiments using human cadavers. The control system assures uniform activation by providing automatic compensation for half-life decay, controls to rotate the body 180° and other controls to stop the irradiation when the two activities equalize. Analog pulse rate techniques are utilized.

Investigator:
E. N. Sheen

INTRODUCTION

In vivo neutron activation experiments, conducted at the University of Washington, in human cadavers by Pacific Northwest Laboratory personnel, required instrumentation to control the irradiation of the body such that uniform activity resulted. Scientists conducting the experiments planned to rotate the body 180° in the neutron flux. This

approach required an automatic system to assure that activity induced after rotation equated to the activity induced before rotation with correction automatically made for the half-life decay of the radionuclide.

The control system described here provides the desired characteristics through utilization of a high accuracy capacitance pulse counter with a shunting resistor calibrated to provide a voltage decay matching the radionuclide decay to within 1% or better. A pulse-rate meter with a very accurate time constant thus serves as the "heart" of the system

*This project was supported in part by the Radiological Physics Section, Radiological Sciences Department.

0012048

DISCUSSION

Figure 1 depicts the circuit diagram of the developed system. Input pulses, derived from neutron flux sensors, connect to a pre-scaler which divides the pulse rate by a factor n and produces an approximate square wave with 10% period variation due to statistical changes of the input rate. The control binary, initially set at $t = 0$, enables AND gate G1 for the pre-scaler output signals and disables G2. Output pulses from G1 drive a saturating transistor switch, Q1, and the collector square wave passes to C2A, the input capacitor of a diode pump. During

positive voltage transitions, current through D2 places charge on C3, a 50 μ F, 200 V, polycarbonate film capacitor. This charge decays through R4 with a current value of $e_{PB}/R4$, where $e_{PB} = ke_0$. Thus, the decay current, $\frac{ke_0}{R4}$, can be adjusted by the variable constant k to calibrate the time constant accurately. Adjustment of e_{PB} (rather than connecting a variable resistor directly across C3) permits R4 to be a fixed, high-value metal film unit (10 M Ω) and R5 to be a much lower value wire-wound potentiometer (10 k Ω to 100 k Ω).

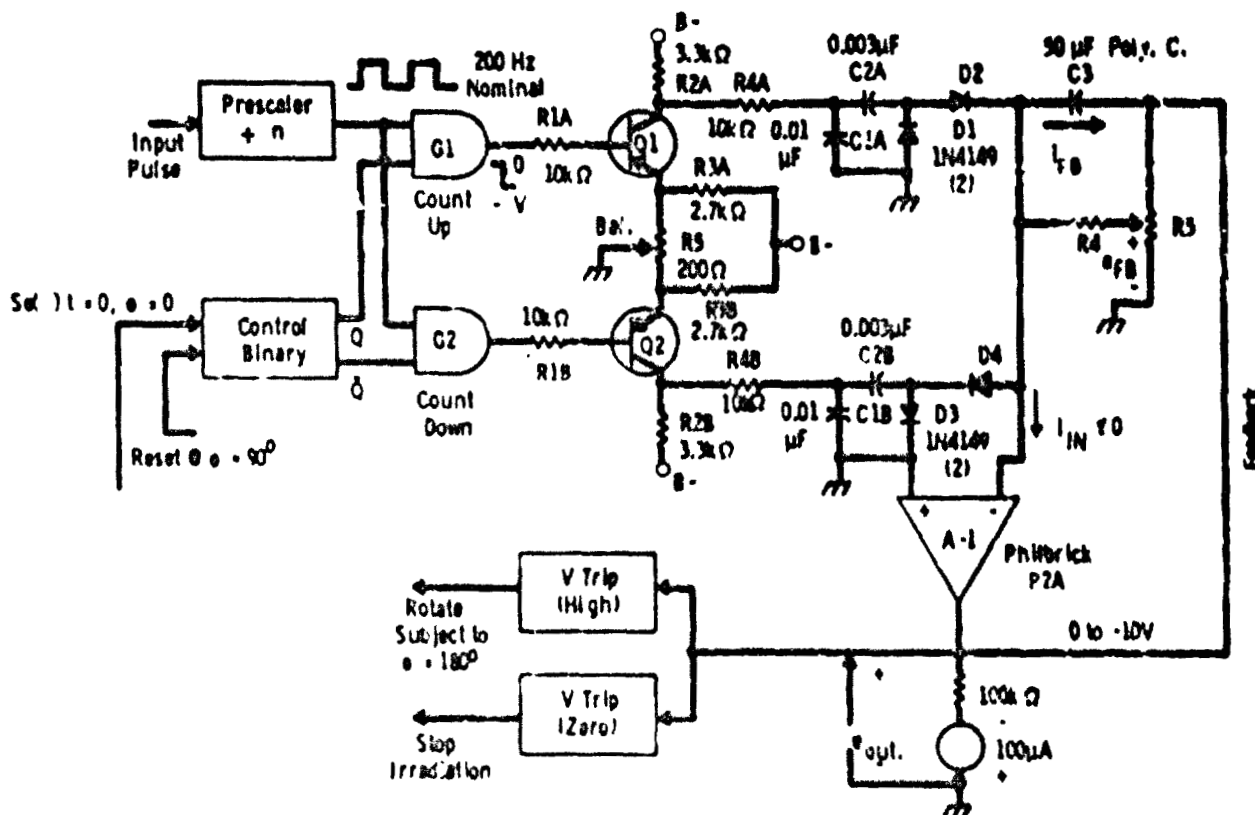


FIGURE 1 - Circuit Diagram

0012049

After sufficient neutron fluence to give $e_0 = V$ trip (high), a signal from the high trip circuit initiates rotation of the irradiated body, and mechanically detected signals reset the control binary at $\theta = 90^\circ$. Pulses then pass through Q2 and remove charge from C3. A second trip circuit provides a signal to stop the irradiation when e_0 crosses zero voltage. These trip circuits operate the necessary relay drivers, etc., to perform the rotation function automatically.

Initial calibration for ^{49}Ca indicated actual voltage decay to match the desired decay (8.83 min

half-life) to within $\pm 0.1\%$. During a 2 hour interval, error due to leakage current measured 0.25 V (R4 removed) or 0.02% full scale per minute. The original design based on 200 Hz nominal input frequency, has operated successfully and accurately for approximately one year.

ACKNOWLEDGEMENT

The author thanks H. Earl Palmer of Radiological Physics Section for envisioning the needs and requirements for the developed system and for his cooperative effort in the tests and application.

SMOKING CONTROL UNIT FOR CANINES*

Uranium miners exposed to radon gas, radon daughters and uranium ore dust in the course of their work, often smoke as well. A study in progress hopes to determine the incidence of lung cancer from any or all of the contaminants and the correlation of one to another. This paper describes an automatic nine-channel system capable of controlling the air-smoke ratios of 1-10 breaths of air to one breath of smoke filled air with beagle dogs. Each dog controls his smoke volume by demand regulation, thus preventing serious distress problems in sensitive animals. The nine-channel unit comprises the previously described three-channel unit extensively modified and a newly designed six-channel unit.

Investigator:
R. L. Wilbur
Technical Assistance:
J. N. Frame, Jr.
J. W. Carmack

INTRODUCTION

A new experimental program, requiring several channels of smoking control, prompted development of a multichannel system which overcame the disadvantages found in the early system⁽¹⁾ and which incorporated new experimental requirements. Extensive modifications became necessary to update the three-channel system to complement the newly designed six-channel unit.

Review of the results of the early experimental work indicated several items which had to be altered to provide more accurate data and to more nearly simulate smoking in man. To satisfy the experimental scope, the new system should:

- Sense tidal volumes in the range of 50 cc to 300 cc.
- Hold the cigarette as close to the canine's mouth as possible.
- Maintain airtight masks around the face.
- Use solenoid air valve with positive closure to prevent smoke from creeping into mask on each breath of air.
- Vent exhaled air through ports, not through the cigarette.
- Minimize dead air space in the mask assembly.
- Provide masks easily disassembled for cleaning and repair.
- Prevent canines from anticipating the inhalation of smoke.
- Include solenoids operating quietly without excessive temperature rise.

Using the above requirements, design and fabrication of a nine-channel system followed. This system can best be described physically as a single unit, stressing system

*This development was supported by funds from the Inhalation Toxicology Section, Biology Department.

operator, and component placement. Electronically, system description focusses on a single channel basis with the aid of a block diagram. Discussion of the methods used to facilitate the requirements summarize the system.

DISCUSSION

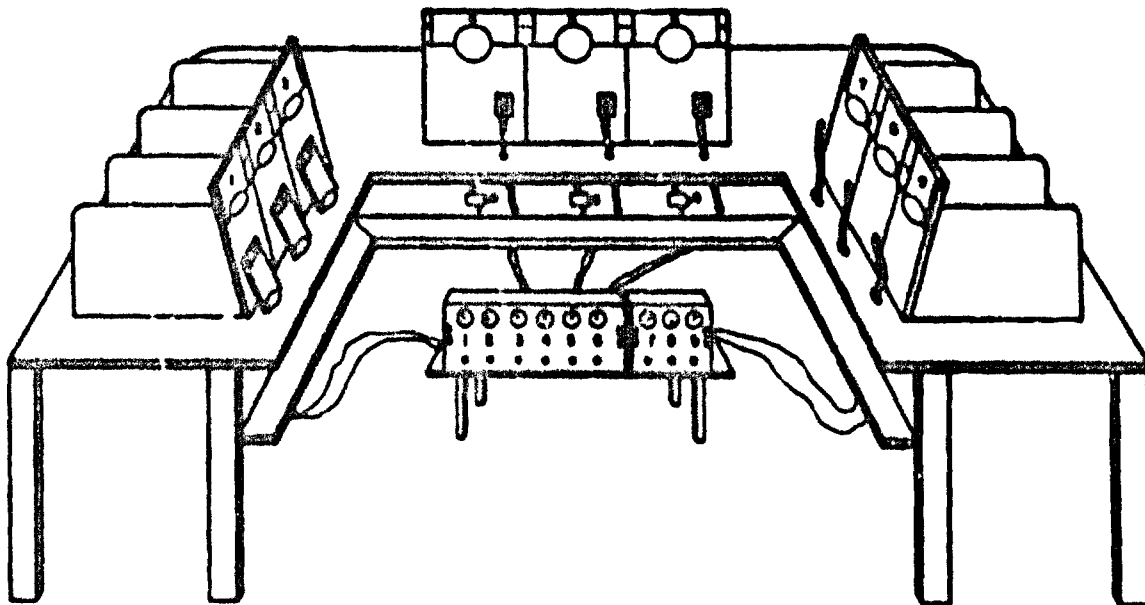
System Description

Figure 1 illustrates the nine-channel system arranged in a "horse-shoe" configuration. Since the mask assemblies, sensors and wiring, and power assemblies would clutter the figure if shown for each position, the various components appear only for description. Positions 1-3 illustrate the mask holder attached to the lower front of the pillory board

in the Down Position. Attachment of the mask assembly in this manner restricts lateral movement, preventing possible damage to the mask by the dog's attempts to free himself from the system. As the mask assembly weighs approximately one pound, the holder serves a support function as well.

Positions 4-6 on the center pillory board, Figure 1, depict the 28 volt power connections for the rotary solenoid and the alarm light. This light energizes momentarily as the rotary solenoid energizes. If the equipment fails or apnea occurs during the smoke breath, the light remains on to alert the operator of a distress condition.

Tygon tubing, which conveys



0012052

FIGURE 1 - 9-Channel Smoking System

pressure signals to the sensors, appears in front of the 7-9 pillory board. Nylon connectors fitted into the table top facilitate tubing replacement when necessary. The pressure sensors, located on the back of the lower shelf, are shown mounted center front.

Both control units, centrally located on a low table, provide access for operation and maintenance. Hence, signal and control cables remain under the table and out of the way at all times.

The "horseshoe" configuration permits nine dogs to smoke simultaneously with only one handler and one operator. The handler, operating from the back of the table, places the dogs in their stalls and remains there during exposure to assist any dog in distress. The operator inside the "horseshoe" inserts, lights, and changes cigarettes as needed. He also monitors the electronic circuits and alarm lights.

After the dog has been secured in the pillory, the handler fits the mask assembly over the dog's mouth and nose. Ties secured behind the head hold the mask in place. The smoking cycle begins by inserting a cigarette into the holder, selecting the proper breath ratio on the control unit and engaging the manual reset to start the dog with air

rather than with smoke. After each animal takes the denoted number of air breaths, the solenoid energizes permitting him to take one smoke breath prior to channel resets and recycle.

Channel Operation

Channel operation can best be described with the block diagram, Figure 2. As the dog inhales air through the mask and the lower venturi, a negative pressure (approximately 0.4 in. H₂O) excites the pressure switch which generates an approximate square wave at the input of the counter driver. The counter driver delays the signal until the end of the inhalation cycle then shapes the pulse to make it compatible with the binary counter.

The 4-bit binary counter, comprised of four integrated circuit clocked flip-flops, uses binary coded

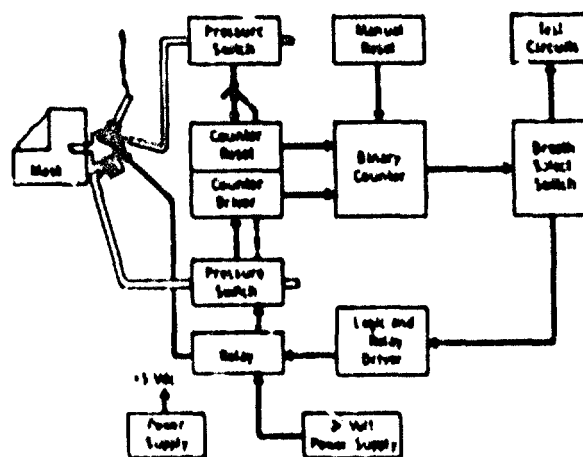


FIGURE 2 - Channel Block Diagram

decimal (BCD) 1-2-4-8 logic. The Breath Select Switch chooses the desired number of counts from 1-10 and sets a quad-input NAND gate. When all NAND gate inputs correspond to the switch setting, the gate produces the logic signal to activate the relay driver.

Upon actuation, the relay applies 28 volts to the mask-mounted rotary dc solenoid and also sets the counter reset circuit. With the solenoid energized, the dog's next inhalation passes through the cigarette and its venturi thus activating the pressure switch and creating the reset signal. Inverted and squared by the counter reset circuitry, this signal resets the binary counter. Simultaneously, the rotary solenoid deenergizes, shutting off the smoke, and the dog resumes breathing air.

Test circuits enable the operator to monitor the signal conditioning portion (pressure switch, counter driver, and binary counter) of any chosen channel with a meter.

Mask Design

The mask now utilized evolved after many attempts to correct air leaks, smoke leakage, dead air space, cigarette position and sensor location problems. It comprises two major subassemblies which join together to form an integral unit.

The face-fitting portion of the mask appears as a 4 in. long cylinder, 3 in. diam, cut as shown in Figure 3. A rubber glove and latex seal formed around the back (A) provide airtight seals about the dog's head. Gauze ties (B) secure the mask to the head. The mouth fits around the mouthpiece (C), insuring that the inhaled air will enter through the flapper valve subassembly. A low resistance exhale valve (D) rapidly vents smoke and air from the mask. Since some dogs salivate excessively during the experiments, a small stopper (E) may be removed periodically to drain saliva from the mask.

The flapper valve assembly consists of a valve housing (F), mounting bracket (G), and rotary solenoid (H). The intake manifold, through which a dog breathes via the mouthpiece, has a 45° included angle, while the rotary solenoid travels through 67°. This assists in achieving a tight closure on the flapper valve. The lower side of the housing holds the air port and venturi (J), where breath counting signals originate. The cigarette holder-venturi (K) attaches to the top of the manifold.

Actuation of the rotary solenoid (H) transmits torque to the flapper valve (L) through the Tygon

coupler (M). Actuation power enters through wires (N), which connect to the 28 volt power connector, Figure 1.

RESULTS AND CONCLUSIONS

Overall system operation may be said to be satisfactory; however, modifications to the mask and counter may be forthcoming as experimental data warrant.

Presently, the system sensitivity requires approximately 50 cubic centimeters (cc) of air per breath to actuate the transducers. This sensitivity depends on the diameter of the venturi. A more sensitive system requires a smaller venturi. Work functions limit the venturi dimensions when the orifice becomes too small for the dog to breath comfortably.

To simulate smoking in man, the cigarette should be as close to the dog's mouth as possible. A previous mask held the cigarette approximately 2-3 inches away from the mouth; this mask moves the cigarette to within 1/2 in. of the mouth.

To assure proper operation of the control system and insure that the dog inhales through the cigarette when the solenoid energizes, the mask must be airtight, as accomplished by the described rubber

seal. A tight fit of the flapper valve in either position insures that no smoke enters on air breaths and that a smoke breath cannot be bypassed by a leaky flapper valve. Exhalation poses no problem with the use of a low resistance exhale valve.

The original experimental system contained a dead air space of volume sufficient to permit shallow-breathing dogs to breathe from this space, inhaling deeply only occasionally. With the respiration rate effectively reduced, the sensor failed to count properly, thus allowing the cigarette to burn down essentially unsmoked. This problem has been greatly reduced by removing all air hoses, bringing the nose and mouth closer to the flapper valve, and slightly reducing the diameter of the mask.

In the earlier system, the solenoid actuated with such force and noise that the dogs learned in short periods of time that the breath following the noise would contain smoke and took action to beat the system. The rotary solenoids circumvent this problem with rotary rather than piston travel and padded rather than metal valves.

This new system minimizes the problems encountered in the earlier system and seems to be suitable for the experimental scope of the pro-

gram. As experiments proceed, there will probably be new problems requiring engineering attention. The design provides versatility sufficient to permit simple incorporation of minor changes in minimal time.

REFERENCE

1. D.P. Brown and N.S. Porter. "Instrument for the Automatic Regulation of Inhaled Aerosols", Hanford Radiological Sciences Research and Development Annual Report for 1966, Vol. V, Instrumentation, BNWL-36V, pp. 5.39-5.42. Pacific Northwest Laboratory, Richland, Washington, January 1965.

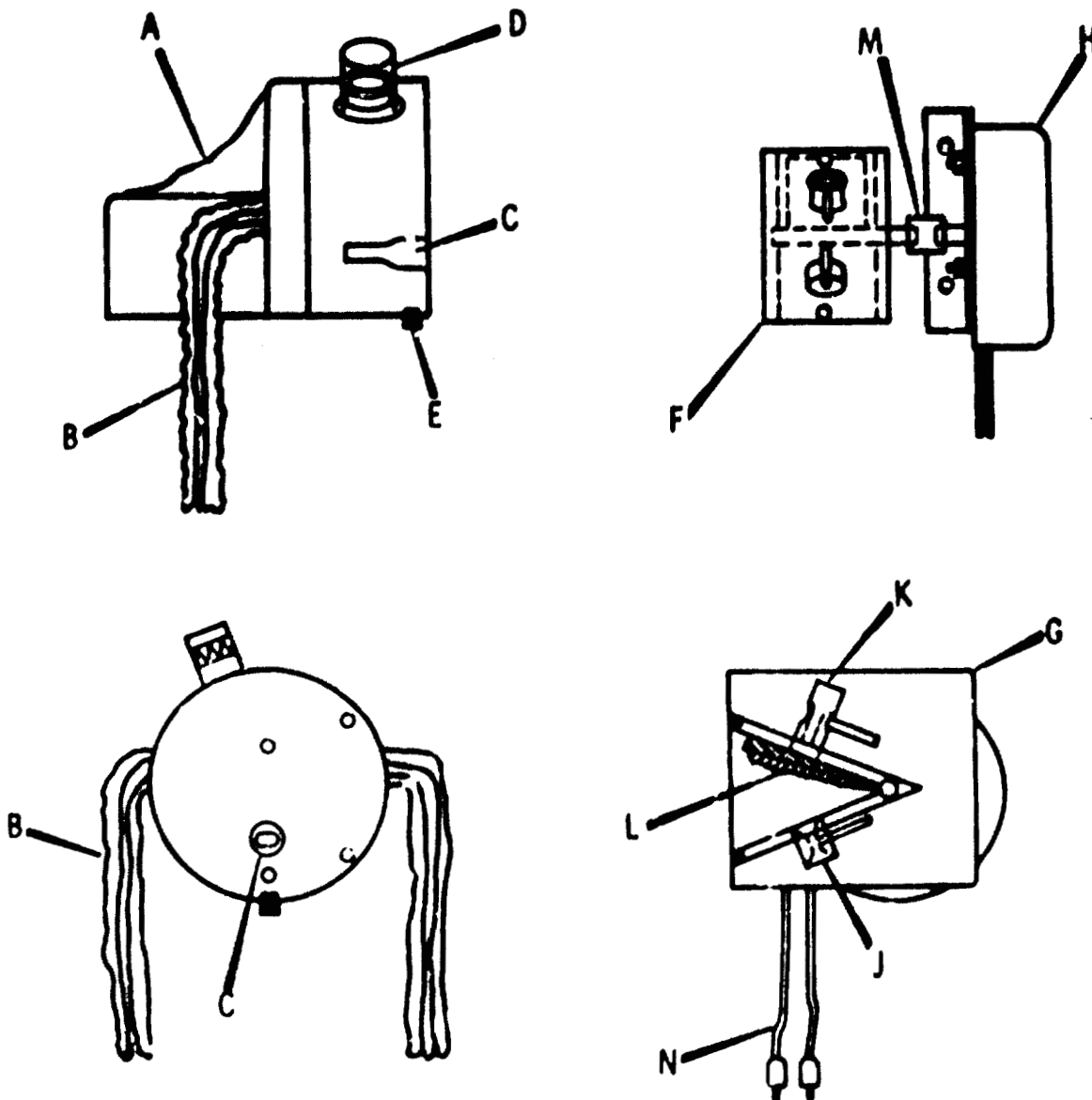


FIGURE 3 - Mask Assembly

0012056

PUBLICATIONS AND PRESENTATIONSDOCUMENTS

Hoitink, N. C. "The Effect of ⁶⁰Co Irradiation of Passivated and Non-passivated Avalanche Diodes Biased Near Breakdown," BNWL-788. December 1968.

Staff of Instrumentation Section, Applied Physics and Electronics Department. Pacific Northwest Laboratory Annual Report for 1967 in the Physical Sciences. BNWL-714, Vol. II: Part 1, June 1968. Pacific Northwest Laboratory, Richland, Washington.

OPEN LITERATURE PUBLICATIONS

Hoitink, N. C., Philipp, L. D., Swinth, K. L. "Compton Suppression Using Pulse Shape Discrimination and Anticoincidence Techniques," IEEE Trans. Nuc. Sci., Vol. NS-15 (3), p. 486. 1968.

Hoitink, N. C. and Sheen, E. M. "Instrument for Reading Ionization Chamber Dosimeter," Med. Res. Engr., Vol. 7 (2), pp. 38-42. 1968.

Philipp, L. D. and Lawritzen, P. "Irradiation Damage to MOS-FETS Operating in the Common Source Mode", IEEE Trans. Nuc. Sci., Vol. NS-14, (6), pp. 284-292. December 1967.

Sheen, E. M., Ratcliffe, C. A., and Glass, W. A. "Beam Current Regulator." Rev. Sci. Instr., Vol. 39 (9), pp. 1261-1265. 1968.

Swinth, K. L. "Measurement of the Photon to Alpha Ratio for Plutonium Isotopes," pp. 279-289. In: Paul Polishuk (Ed.) Nucleonics in Aerospace, Proceedings of the Second International Symposium held in Columbus, Ohio, July 12-14, 1967. Plenum Press, New York. 1968.

Swinth, K. L. "Interpreting Counting Data From Internally Deposited Plutonium," p. 208. In: Diagnosis and Treatment of Deposited Radionuclides, Excerpta Medica Foundation, Amsterdam, 1968.

PRESENTATIONS AT SOCIETY MEETINGS AND SYMPOSIA

Swinth, K. L., Philipp, L. D., and Hoitink, N. C. "Compton Suppression Using Pulse Shape Discrimination and Anticoincidence Techniques," Eleventh Scintillation and Semiconductor Counter Symposium, Washington, D.C., February 28 - March 1, 1968.

Swinth, K. L. and Bair, W. J. "The Retention of Inhaled Plutonium in Dogs". Thirteenth Annual Meeting of the Health Physics Society, Denver, Colorado, June 17-20, 1968.

Swinth, K. L. "Wound Counting With Solid State Detectors". Thirteenth Annual Meeting of the Health Physics Society, Denver, Colorado, June 17-20, 1968.

END

DATE FILMED

10 / 22 / 69

0012058